RADC-TR-87-158
Final Technical Report
May 1988

A HYBRID-ITERATIVE APPROACH FOR RCS MODELING ON SUPER COMPUTERS

The University of Dayton

G. A. Thiele, P. K. Murthy and R. P. Penno

ROME AIR DEVELOPMENT CENTER
Air Force Systems Command
Griffiss AFB, NY 13441-5700

This report has been reviewed by the RADC Public Affairs Office (PA) and is releasable to the National Technical Information Service (NTIS). At NTIS it will be releasable to the general public, including foreign nations.

RADC-TR-87-158 has been reviewed and is approved for publication.

APPROVED: Robert V McGahan

ROBERT V. McGAHAN
Project Engineer

APPROVED:

PAUL J. FAIRBANKS, Lt Colonel, USAF
Deputy Director of Electromagnetics

FOR THE COMMANDER: John A. Ritz

JOHN A. RITZ
Directorate of Plans & Programs

If your address has changed or if you wish to be removed from the RADC mailing list, or if the addressee is no longer employed by your organization, please notify RADC (EECT) Hanscom AFB MA 01731-5000. This will assist us in maintaining a current mailing list.

Do not return copies of this report unless contractual obligations or notices on a specific document require that it be returned.

UNCLASSIFIED

SECURITY CLASSIFICATION OF THIS PAGE

REPORT DOCUMENTATION PAGE

Form Approved OMB No. 0704-0188

1a. REPORT SECURITY CLASSIFICATION UNCLASSIFIED	1b. RESTRICTIVE MARKINGS N/A
2a. SECURITY CLASSIFICATION AUTHORITY N/A	3. DISTRIBUTION/AVAILABILITY OF REPORT Approved for public release; distribution unlimited.
2b. DECLASSIFICATION/DOWNGRADING SCHEDULE N/A	
4. PERFORMING ORGANIZATION REPORT NUMBER(S) UDR-TR-86-133	5. MONITORING ORGANIZATION REPORT NUMBER(S) RADC-TR-87-158
6a. NAME OF PERFORMING ORGANIZATION The University of Dayton Graduate Engineering & Research 6b. OFFICE SYMBOL (If applicable)	7a. NAME OF MONITORING ORGANIZATION Rome Air Development Center (EECT)
6c. ADDRESS (City, State, and ZIP Code) School of Engineering 300 College Park, KL 262 Dayton OH 45469-0001	7b. ADDRESS (City, State, and ZIP Code) Hanscom AFB MA 01731-5000
8a. NAME OF FUNDING/SPONSORING ORGANIZATION Rome Air Development Center 8b OFFICE SYMBOL (If applicable) EECT	9 PROCUREMENT INSTRUMENT IDENTIFICATION NUMBER F19628-83-K-0034
8c. ADDRESS (City, State, and ZIP Code) Hanscom AFB MA 01731-5000	10. SOURCE OF FUNDING NUMBERS PROGRAM ELEMENT NO: 62702F; PROJECT NO: 4600; TASK NO: 15; WORK UNIT ACCESSION NO: 68

11. TITLE (Include Security Classification)
A HYBRID-ITERATIVE APPROACH FOR RCS MODELING ON SUPER COMPUTERS

12. PERSONAL AUTHOR(S)
G.A. Thiele, P.K. Murthy, R.P. Penno

13a. TYPE OF REPORT	13b TIME COVERED	14. DATE OF REPORT (Year, Month, Day)	15 PAGE COUNT
Final	FROM Dec 83 TO Oct 86	May 1988	74

16. SUPPLEMENTARY NOTATION
N/A

17. COSATI CODES			18. SUBJECT TERMS (Continue on reverse if necessary and identify by block number)
FIELD	GROUP	SUB-GROUP	Hybrid-iterative method (HIM) RCS Modeling Edge diffraction theory
17	09		
17	11		

19. ABSTRACT (Continue on reverse if necessary and identify by block number)

An iterative method is developed for computing the current induced by plane wave excitation on conducting bodies of arbitrary shape. In this method, the scattering body is divided into lit- and shadow-side regions separated by the geometric optics boundary. An MFIE is written for each region. Each MFIE is solved by iteration (i.e., method of successive substitutions). In order to accomplish this, it is often necessary to have an initial estimate of the shadow side current. This estimate is obtained from edge diffraction theory or Fock theory. Hence, the method is called a Hybrid-iterative method (HIM). The HIM is well-suited for use on a super computer like the Cray XMP. Results will be shown for 2-dimensional objects whose size varies from 0.6 λ to 440 λ, , all with CPU times under one minute.

20 DISTRIBUTION/AVAILABILITY OF ABSTRACT ☒ UNCLASSIFIED/UNLIMITED ☐ SAME AS RPT ☐ OTIC USERS	21 ABSTRACT SECURITY CLASSIFICATION UNCLASSIFIED
22a. NAME OF RESPONSIBLE INDIVIDUAL Robert V. McGahan	22b TELEPHONE (Include Area Code) (617) 377-4239 22c OFFICE SYMBOL RADC (EECT)

DD Form 1473, JUN 86 — Previous editions are obsolete.

SECURITY CLASSIFICATION OF THIS PAGE
UNCLASSIFIED

TABLE OF CONTENTS

LIST OF FIGURES..... iii

SECTION 1

INTRODUCTION..... 1

SECTION 2

GENERAL HIM THEORY..... 4

2.1 MAGNETIC FIELD INTEGRAL EQUATION..... 4

2.2 CURRENTS..... 6

2.3 CONVERGENCE CRITERION..... 8

SECTION 3

INITIAL CURRENTS..... 10

3.1 SHADOW-SIDE CURRENT ON A WEDGE..... 10

3.2 SHADOW-SIDE CURRENT ON A SMOOTH BODY..... 12

SECTION 4

NUMERICAL EXAMPLES..... 20

4.1 SQUARE CYLINDER..... 20

4.2 SCATTERERS WITH SMOOTH SURFACE..... 21

4.3 SCATTERERS WITH A SMOOTH SURFACE JOINED TO AN EDGE.. 34

4.4 VERY LARGE SCATTERERS..... 35

4.5 PERFECTLY CONDUCTING CUBE..... 44

4.6 TM CASE FOR SQUARE CYLINDER..... 44

SECTION 5

SUMMARY..... 59

REFERENCES..... 61

LIST OF FIGURES

FIGURE		PAGE
1.	Scattering by a perfectly conducting body.....	5
2.	Wedge illuminated by a TM-plane wave.....	11
3a.	Shadow side currents on a wedge. $\alpha = 90^0$	13
3b.	Shadow side currents on a wedge. $\alpha = 90^0$	14
4.	Geometry for a square cylinder.....	15
5.	Geometry for a smooth convex cylinder.....	16
6.	Shadow side Fock current on a circular cylinder. Radius 3.2λ, $\phi_i = 90^0$	19
7.	Magnitude of current on a square clyinder. Order = 0, $w = 3.7\lambda$, $\phi_i = 115^0$	22
8.	Phase of current on a square cylinder. Order = 0, $w = 3.7\lambda$, $\phi_i = 115^0$	23
9.	Magnitude of current on a square cylinder. Order = 1, $w = 3.7\lambda$, $\phi_i = 115^0$	24
10.	Phase of current on a square cylinder. Order = 1, $w = 3.7\lambda$, $\phi_i = 115^0$	25
11.	Bistatic echo width of a square cylinder. Order = 1, $w = 3.7\lambda$, $\phi_i = 115^0$	26
12.	Magnitude of current on a square cylinder. Order = 0, $w = 3.7\lambda$, $\phi_i = 95^0$	27
13.	Phase of current on square cylinder. Order = 0, $w = 3.7\lambda$, $\phi_i = 95^0$	28
14.	Magnitude of current on a square cylinder. Order = 2,e $w = 3.7\lambda$, $\phi_i = 95^0$	29
15.	Phase of current on a square cylinder. Order = 2, $w = 3.7\lambda$, $\phi_i = 95^0$	30
16.	Bistatic echo width of a square cylinder. Order = 2, $w = 3.7\lambda$, $\phi_i = 95^0$	31
17.	Magnitude of current on a circular cylinder. Order = 0, Radius = 3.2λ, $\phi_i = 90^0$	32

LIST OF FIGURES (cont'd)

FIGURE		PAGE
18.	Phase of current on a circular cylinder. Order = 0, Radius = 3.2λ, $\phi_i = 90^0$	33
19.	Bistatic echo width of a circular cylinder. Order = 0, Radius $3.2\ \lambda$, $\phi_i = 90^0$	34
20.	Geometry for an elliptic cylinder with semi-major axis "a" and semi-minor "b". $\phi_i = 90^0$	36
21.	Magnitude of current on an elliptic cylinder. Order = 0, a = 1.5λ, b = 1.0λ, $\phi_i = 90^0$	37
22.	Ogival cylinder results for a 3λ long 80^0 ogive with edge-on incidence. Current is zeroth order only. Excellent agreement between HIM and MM.....	38
23.	Same as Figure 22 except incidence is "broadside" and current is second order since this is a more difficult case than edge-on incidence. Note that this is an example of a curved surface joined to an edge.....	39
24.	Large circular cylinder example with a = 25λ. See chart for computer times.....	41
25.	Large circular cylinder example with a = 80λ. See chart for computer times.....	42
26.	Note: $\gamma = 90^0$ Backscatter $\gamma = 270^0$ Forward scatter.....	46
27.	H-plane bistatic scattering from a metal cube 0.75λ on a side.....	47
28.	H-plane bistatic scattering from a metal cube 1.5λ on a side.....	48
29.	H-plane bistatic scattering from a metal cube 3.0λ on a side.....	49
30.	E-plane bistatic scattering from a metal cube of width .775 λ.....	50
31.	E-plane bistatic scattering from a metal cube of width 1.5075 λ	51
32.	E-plane bistatic scattering from a metal cube of width 3.015 λ	52

LIST OF FIGURES (cont'd)

FIGURE..... PAGE

33. E-plane polarized component of initial current on side face - magnitude..... 53

34. E-polarized component of first order current on side face - magnitude..... 53

35. H-polarized component of first order current on front face - magnitude..... 54

36. Cross-polarized component of first order current on side face - magnitude..... 54

37. Magnitude of current on a square cylinder. Order = 4, $w = 3.193\lambda$, $\phi_i = 135^0$ 55

38. Phase of current on a square cylinder. Order = 4, $w = 3.193\lambda$, $\phi_i = 135^0$ 56

39. Magnitude of current on a square cylinder. Order = 4, $w = 3.193\lambda$, $\phi_i = 120^0$ 57

40. Phase of current on a square cylinder. Order = 4, $w = 3.193\lambda$, $\phi_i = 120^0$ 58

SECTION 1
INTRODUCTION

The technique that has evolved from this research effort is called HIM which stands for Hybrid Iterative Method. It is the third generation of a technique that was initially researched when Dr. G. A. Thiele was with the Ohio State University ElectroScience Laboratory. This evolution is described below.

Starting in 1979, Kim and Thiele developed a hybrid AS-MM technique (asymptotic moment-method technique) to find the induced currents on the surface of scatterers in the intermediate frequency region [1]. These induced currents consisted of two parts: an "optics" current similar to (but not the same as $2\hat{n} \times \bar{H}^i$); and a "correction" current which was the difference between the optics current and the true current. The correction current was obtained via the moment method.

In 1983 and 1984, Kaye, Murthy and Thiele [2], [3] significantly improved on the AS-MM work by eliminating the moment method regions thereby making the method potentially applicable to large scatterers as well as ones of modest size. In the second generation work by Kaye, Murthy and Thiele, the magnetic field integral equation (MFIE) was reduced to a sequence of integral equations for both the "optics" currents and the "correction" currents, <u>each</u> of which is solved by iteration. On the other hand, in Kim and Thiele [1], the "correction" currents were solved by the moment method which tends to limit the electrical size of the object that may be considered. The second generation work, then, was a purely iterative technique wherein all the integral equations (for both the optics currents and the correction currents) are of the same form and are similarly solved via iteration.

In 1985 and 1986, Murthy, Hill and Thiele [4], [5] evolved the third-generation technique, which is the present technique and which is described in the next section. This third-generation technique is called HIM for Hybrid Iterative Method. In HIM, we incorporate the correction currents into the ansatz for the iterative scheme itself so that there is only one current to iterate. Thus, the iterative solution proceeds by taking the previously iterated current and using it as the "new" current to be improved upon. Typically, ten iterations is sufficient to obtain a converged correct current. The second- and third-generation techniques were mostly supported by RADC/Hanscom.

The salient features of the hybrid-iterative method (HIM) may then be stated in the following way. HIM is an iterative algorithm to solve MFIE (magnetic field integral equation) for induced surface currents on a scatterer. Every iterative scheme must be started with an initial guess. The better the initial guess, the faster the method converges. This initial guess must be obtained from a knowledge of the physics of the scattering process to the extent it is known. Thus, in HIM, the physics of the scattering process is incorporated into the solution process at the outset to the extent it is possible, in the form of an initial guess for the current on the shadow side. This results, directly, in the reduction of CPU time. It is to be noted that the iteration method [2], [3] is a special case of HIM in that it takes the shadow-side current to be zero. For some scattering geometries, such a crude initial guess may not be good enough to warrant a converged solution. In HIM, the solution always converges when the initial guess is other than zero.

In Section II, we develop the integral equations for HIM and discuss their solution by iteration. In Section III, we present theory relevant to the initial estimates of the shadow-side currents for both smooth and edged bodies. Section IV presents calculated results using the theory developed in Section II. Both edged bodies, exemplified by a square cylinder and smooth

bodies, exemplified by circular and elliptic cylinders are considered. Section IV also presents our results obtained on the Cray X-MP. In addition, ogival cylinders which involve both edge- and smooth-surface diffraction, and hence constitute a stricter test of the method, are also considered. Section V contains the summary of the technique and points out further avenues of research.

SECTION 2
GENERAL HIM THEORY

2.1 MAGNETIC FIELD INTEGRAL EQUATION

Consider a perfectly conducting body illuminated by a plane wave. The induced surface current density on the body at an observation point P, as shown in Figure 1, can be computed from the MFIE:

$$\vec{J}(\vec{R}) = 2\hat{n} \times \vec{H}_i(\vec{R}) + 2\hat{n} \times L[\vec{J}] \tag{1}$$

where the operator L is defined by

$$L[\vec{J}] = \int_{\Sigma} \vec{J}(\vec{R}') \times \vec{\nabla}' G(r)\, ds' \quad . \tag{2}$$

The surface of the body is denoted by Σ and $\vec{R}$ and $\vec{R}'$ are the observation and source point position vectors, respectively, on Σ and $r = |\vec{R} - \vec{R}'|$. The prime on the gradient operator indicates that the differentiation is performed on the source coordinates. The bar through the integral sign is used to denote the principle value integral over Σ. $\vec{H}^i$ is the incident magnetic field vector and $\hat{n}$ is the outward unit normal to the surface at $\vec{R}$. G(r) is the free-space Green's function given by

$$G(r) = \frac{e^{-j\beta r}}{4\pi r} \tag{3}$$

for the three-dimensional problem and by

$$G(r) = \frac{1}{4j} H_o^{(2)}(\beta r) \tag{4}$$

for the two-dimensional problem. $H_o^{(2)}(\beta r)$ is the zero-order Hankel function of the second kind and β is the free space propagation constant. The time dependence is taken to be $\exp(j\omega t)$ and is suppressed throughout.

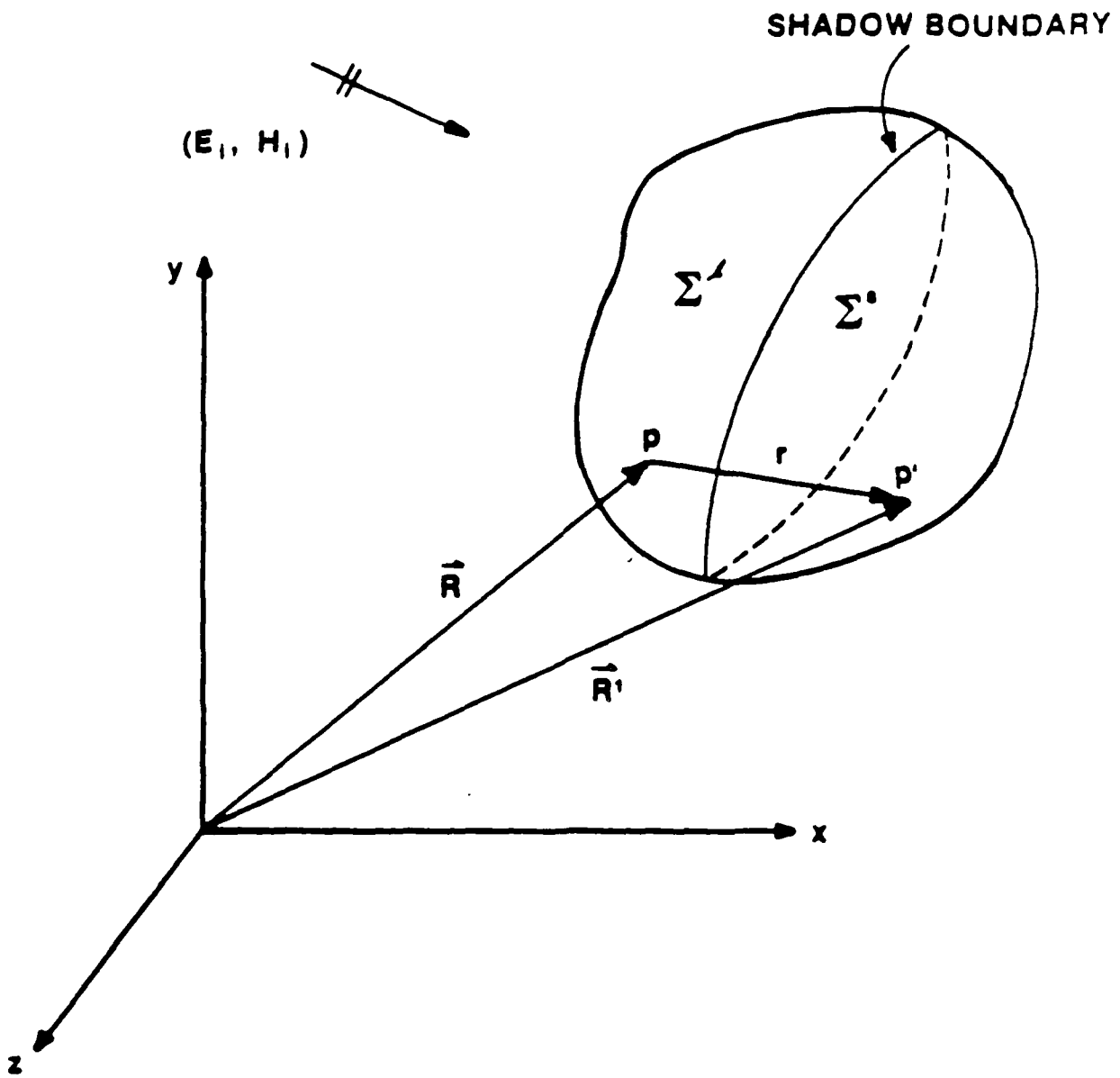

Figure 1. Scattering by a perfectly conducting body.

2.2 CURRENTS

The first step in solving the MFIE for the induced surface current density $\vec{J}(\vec{R})$ is to divide the total surface Σ of the body into Σ^{ℓ} and Σ^{s}, which represents the lit and shadowed regions, respectively. The dividing line between these two regions is the geometrical optics shadow boundary which is defined as the locus of points satisfying $\hat{u} \cdot \hat{n} = 0$, where $\hat{u}$ is the unit vector in the direction of propagation of the incident field. Then $\vec{J}(\vec{R})$ can be expressed as follows:

$$\vec{J}(\vec{R}) = \delta\vec{J}^{\ell}(\vec{R}) + (1 - \delta)\vec{J}^{s}(\vec{R}) \tag{5}$$

where $\delta=1$ if $\vec{R} \in \Sigma^{\ell}$ and $\delta=0$ if $\vec{R} \in \Sigma^{s}$. Eq. (1) can now be rewritten as

$$\vec{J}(\vec{R}) = 2\hat{n} \times \vec{H}_i(\vec{R}) + 2\hat{n} \times L[\vec{J}^{\ell}] + 2\hat{n} \times L[\vec{J}^{s}] \ . \tag{6}$$

In the notation used in Eq. (6) and in subsequent equations, the surface of integration is identified by the superscript on the current density. We now write out Eq. (6) explicitly for $\vec{R} \in \Sigma^{\ell}$ and $\vec{R} \in \Sigma^{s}$:

$$\vec{J}^{\ell}(\vec{R}) = 2\hat{n} \times \vec{H}_i(\vec{R}) + 2\hat{n} \times L[\vec{J}^{\ell}] + 2\hat{n} \times L[\vec{J}^{s}] \tag{7}$$

$$\vec{J}^{s}(\vec{R}) = 2\hat{n} \times \vec{H}_i(\vec{R}) + 2\hat{n} \times L[\vec{J}^{\ell}] + 2\hat{n} \times L[\vec{J}^{s}] \tag{8}$$

The problem of solving for the induced surface current density has now been transformed into one of solving Eqs. (7) and (8) for $\vec{J}^{\ell}$ and $\vec{J}^{s}$. We compute these currents in sequential fashion in the following way.

First, let $\vec{J}^{s}_{E}$ be an estimate of shadow current. For edged bodies like the square cylinder, this current is obtained from the wedge diffraction theory. For smooth bodies like circular or elliptic cylinders, this current is obtained using Fock theory.

A detailed discussion of determining $\underline{J}^s_E$ will be considered in Section III. Thus,

$$\underline{J}^s \sim \underline{J}^s_E \tag{9}$$

Substituting Eq. (9) in Eq. (7) and noting that the current on the lit side would now be an approximation to the true current and denoting this zeroth order approximate current by $\underline{J}^\ell_o$,

$$\underline{J}^\ell_o(\underline{R}) = 2\hat{n} \times \underline{H}_i(\underline{R}) + 2\hat{n} \times L[\underline{J}^\ell_o] + 2\hat{n} \times L[\underline{J}^s_E] \tag{10}$$

This current is a significant improvement over the classical physical optics (PO) current since it takes into account mutual interaction of current on both lit- and shadow-regions in addition to the geometrical optics (GO) field.

A shadow-side zeroth order approximate current, $\underline{J}^s_o$, is now defined by substituting $\underline{J}^\ell = \underline{J}^\ell_o$ in (8):

$$\underline{J}^s_o(\underline{R}) = 2\hat{n} \times \underline{H}_i(\underline{R}) + 2\hat{n} \times L[\underline{J}^\ell_o] + 2\hat{n} \times L[\underline{J}^s_o] \tag{11}$$

In this expression, the main contribution of the second term on the right-hand side will be approximately $-2\hat{n} \times \underline{H}_i(\underline{R})$ to cancel the first term. The $\underline{J}^s_o$ obtained from Eq. (11) would be closer to the true current than our initial guess $\underline{J}^s_E$. Indeed, the only inaccuracy incurred being that through the approximate value taken for the lit-side current.

Now that an approximation to the shadow-side current better than $\underline{J}^s_E$ is available, the next higher-order current on the lit side may be obtained. This lit-side current may be used to further improve the shadow-side current. Thus, higher-order currents may be obtained until the desired accuracy is achieved. The integral equations for the nth order currents may be defined as follows:

$$\vec{J}_n^{\ell}(\vec{R}) = 2\hat{n} \times \vec{H}_i(\vec{R}) + L[\vec{J}_n^{\ell}] + L[\vec{J}_{n-1}^{s}] \tag{12}$$

$$\vec{J}_n^{s}(\vec{R}) = 2\hat{n} \times \vec{H}_i(\vec{R}) + L[\vec{J}_n^{\ell}] + L[\vec{J}_n^{s}] \tag{13}$$

$$n = 1, 2 \ldots$$

$\vec{J}_o^{s}$ is the solution of Eq. (11).

In the iterative technique described in an earlier paper [2], the "optics" currents were improved upon by the addition of correction currents. The technique described here is mathematically equivalent to the correction current ansatz of that iterative technique and at the same time is simpler from the programming point of view.

2.3 CONVERGENCE CRITERION

We now give a criterion for the convergence of the sequence of integral equations. This criterion is based upon how accurately our solution satisfies the MFIE. Using Equation (5), we define,

$$\vec{J}_n(\vec{R}) = \delta\, \vec{J}_n^{\ell}(\vec{R}) + (1 - \delta)\, \vec{J}_n^{s}(\vec{R}) \tag{14}$$

Then the current, $\vec{J}_n^{*}(\vec{R})$, is obtained by substituting $\vec{J}_n(\vec{R})$ in MFIE. That is,

$$\vec{J}_n^{*}(\vec{R}) = 2\hat{n} \times \vec{H}_i(\vec{R}) + 2\hat{n} \times L[\vec{J}_n(\vec{R})] \tag{15}$$

If $\vec{J}_n(\vec{R})$ were to be exact, then $\vec{J}_n^{*}(\vec{R}) \equiv \vec{J}_n(\vec{R})$. The "difference" between $\vec{J}_n^{*}(\vec{R})$ and $\vec{J}_n(\vec{R})$ is a measure of the degree of accuracy of the solution after n-orders of iteration. Noting that the currents are specified as a set of N points, the average error, ε, between $\vec{J}_n^{*}$ and J_n is defined to be,

$$\varepsilon_n = \frac{1}{N} \sum_{i=1}^{N} |J^{*}_{n,i} - J_{n,i}|^2 \,^{1/2} \qquad (16)$$

If the error ε_n is less than a preselected value, the sequence may be considered to have converged.

Thus, the hybrid-iterative method (HIM) computes the currents on the lit and shadow regions in sequential fashion starting with an initial estimate for the shadow current. All the integral equations are of the same form and are, in fact, Fredholm integral equations of the second kind. Hence, all these integrals may be solved by iteration as discussed in [2], [3].

SECTION 3
INITIAL CURRENTS

An initial estimate of the current on a scatterer with surface discontinuities like a square cylinder is obtained from the knowledge of currents on a wedge. For a scatterer with smooth surface, Fock theory may be used to obtain the initial estimate of the shadow-side current.

3.1 SHADOW-SIDE CURRENT ON A WEDGE

Consider the wedge shown in Figure 2 illuminated by a TE-plane wave. When the angle of incidence ϕ_i is such that the shadow boundary is not "close" to face B, the current on face B is given by [5]

$$\underline{J}_E^s = -4\frac{H_o}{N} K_-(x_B)\, e^{-j\beta\rho}\, \hat{t}_B, \quad \begin{matrix} 0 \le \rho \le \infty \\ 0 \le \phi_i \le (n-1)\pi - \frac{n\pi}{10} \end{matrix} \tag{17}$$

where

$$K_-(x) = \sqrt{\frac{j}{\pi}}\, e^{jx^2} \int_x^\infty e^{-jt^2}\, dt$$

$$x_B = \sqrt{2\beta\rho_B}\quad (\cos\frac{\pi}{n} + \cos\frac{\phi_i}{n})/\sin\frac{\pi}{n}$$

H_o = amplitude of the incident magnetic field

ρ = distance from the edge

$n = (2 - \frac{\alpha}{\pi})$

α = interior wedge angle.

When the angle of incidence is such that a shadow boundary is close to Face B, the current is given by,

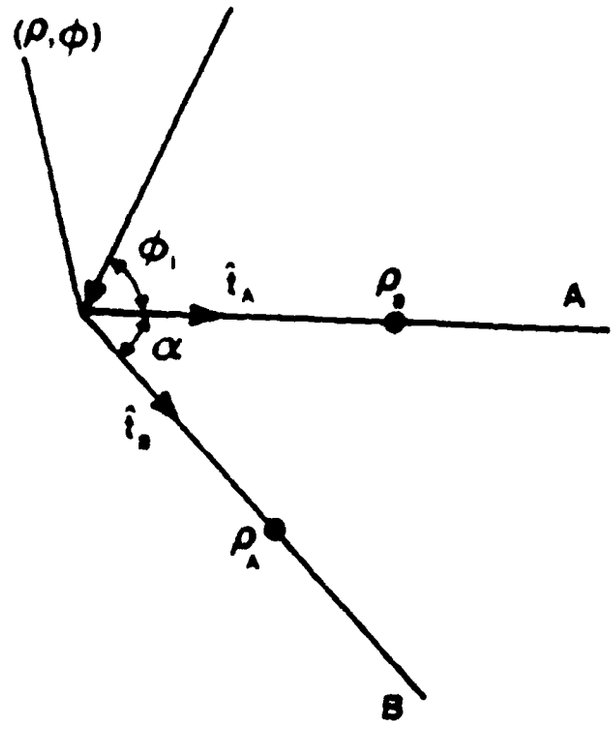

Figure 2. Wedge illuminated by a TM-plane wave.

$$\vec{J}_E^s = -2H_o[B\,K_-(Bx_B^-) + \mathrm{sgn}(\cot\psi^+)\,K_-(x_B^+)]\,e^{-j\beta\rho}\,\hat{t}_B\ , \qquad (18)$$

$$0 \leq \rho \leq \infty$$

$$(n-1)\pi - \frac{n\pi}{10} \leq \phi_i \leq (n-1)\pi$$

where $B = (\frac{2}{n} - 1)$

$$x_B = \sqrt{\beta\rho/2}\quad 2n\cot\psi$$

$$\psi = (\pi \mp \phi_i)/2n$$

Thus, Equations (17) and (18) express the currents on the shadow side of a wedge in closed form. These expressions involve the well-known modified Fresnel functions, $K_-(x)$ [6], and are easy to compute. Figure 3 presents shadow-side currents on wedge computed using the above expressions as well as the exact solution obtained from the eigenfunction solution. Note that the agreement is excellent.

These currents on the wedge may readily be used to obtain an initial estimate of the shadow-side current on a square cylinder. Consider the geometry of a square cylinder shown in Figure 4. Faces 2 and 3 are in the shadow region. Faces 1 and 2 constitute a wedge illuminated with the angle of incidence being $\phi_{i,B}$. The current on Face 2 may be approximated by the current on a corresponding wedge with $\alpha = \pi/2$ and $\phi_i = \phi_{i,B}$. In a similar fashion, the current on Face 3 also may be approximated.

3.2 SHADOW-SIDE CURRENT ON A SMOOTH BODY

An estimate for current on the shadow side of a smooth convex cylinder may be obtained by using Fock theory [4]. Referring to Figure 5, Q_1 and Q_2 are points of grazing incidence and Q_0 is the observation point where current is to be found. The field at Q_0 is due to two creeping waves launched from Q_1 and

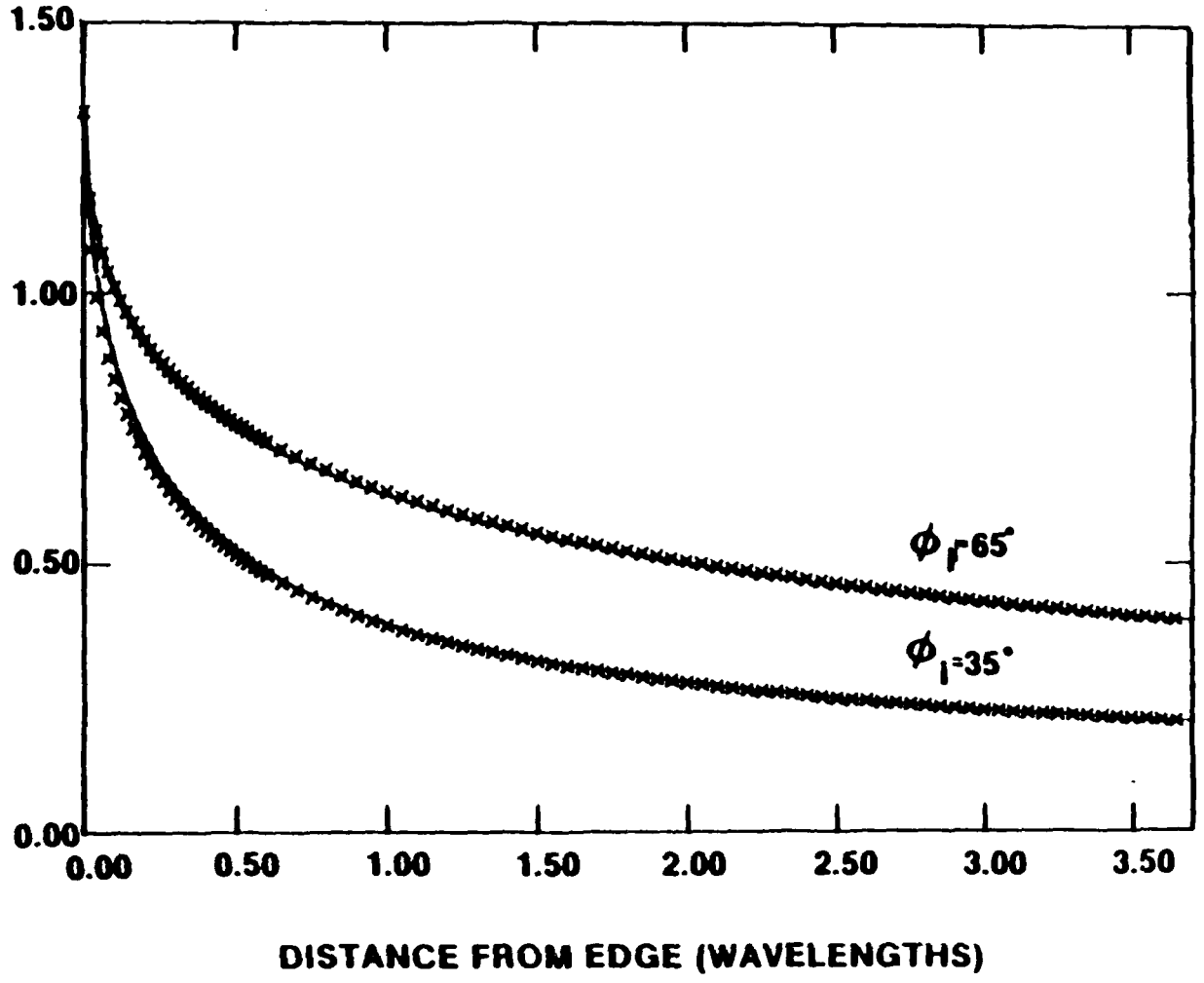

Figure 3a. Shadow side currents on a wedge. $\alpha = 90^0$

_____ Exact Solution

x x x x Closed Form Solution

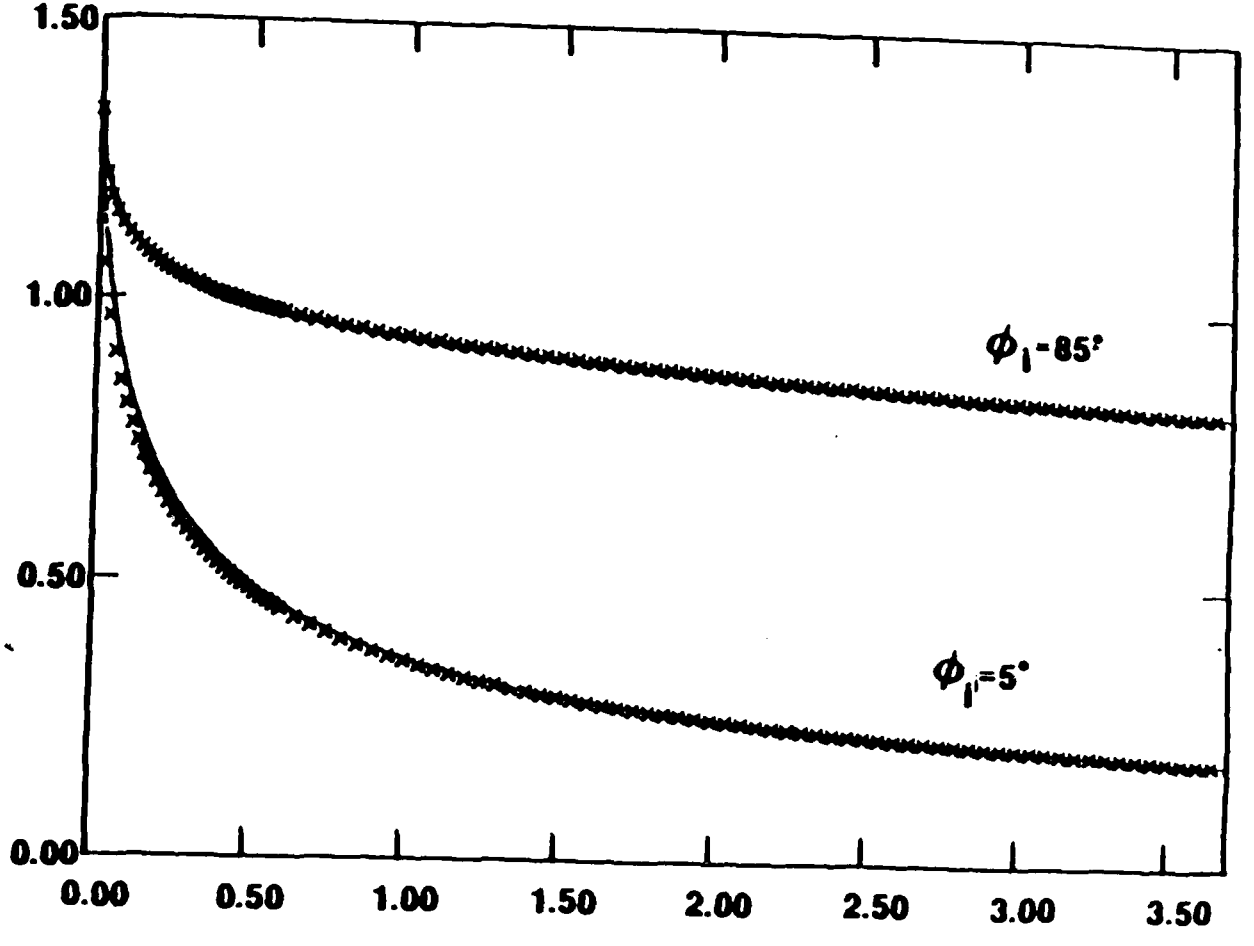

Figure 3b. Shadow side currents on a wedge. $\alpha = 90^0$

———— Exact Solution

x x x x Closed Form Solution

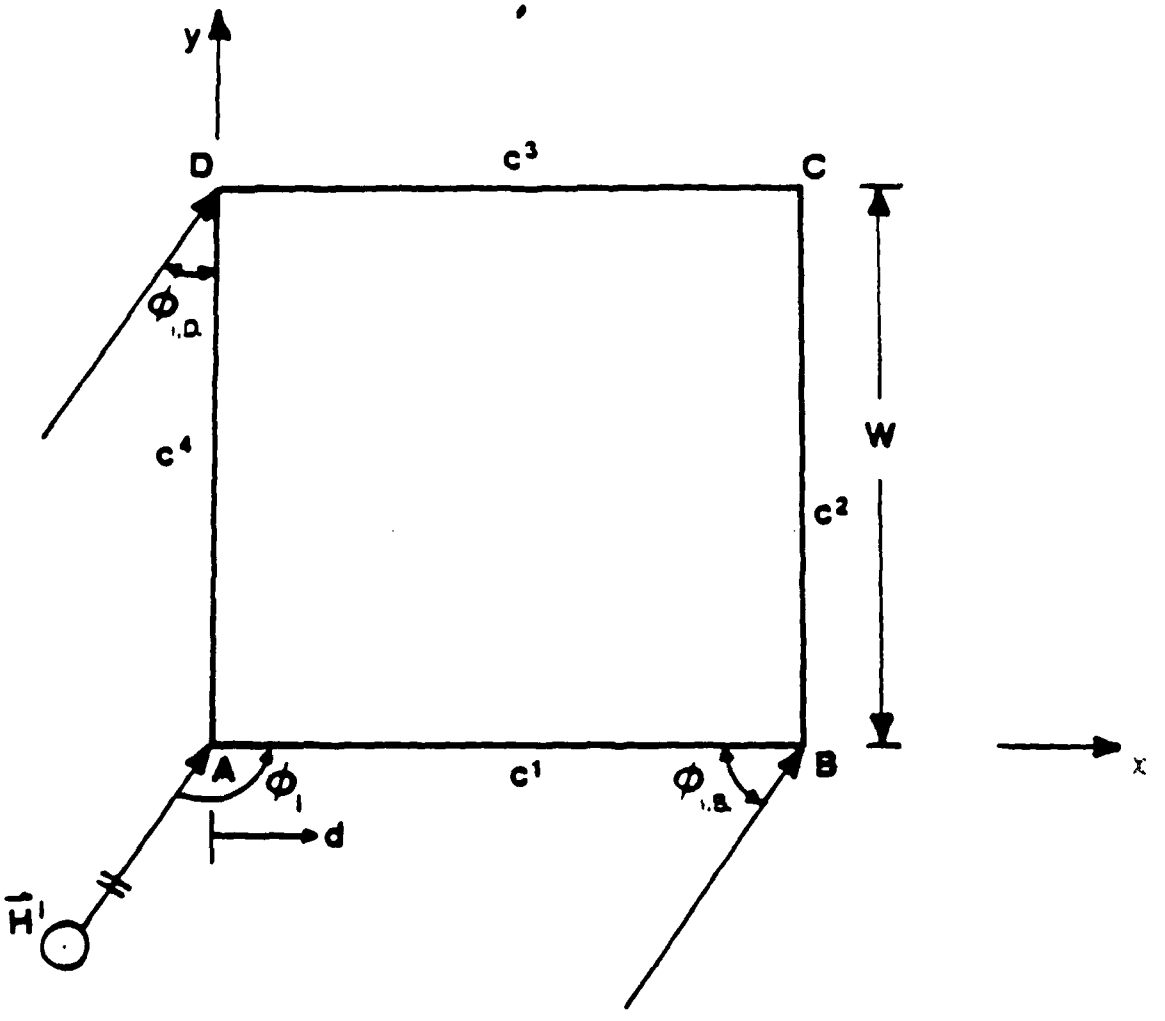

Figure 4. Geometry for a square cylinder.

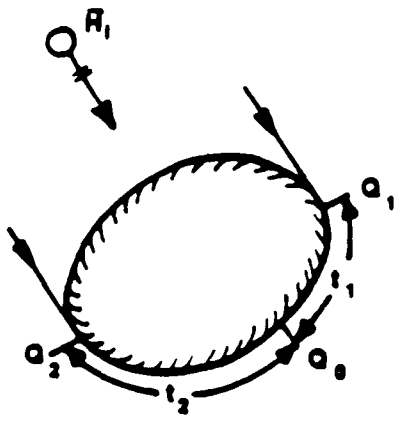

Figure 5. Geometry for a smooth convex cylinder.

Q_2 and traveling the distance of t_1 and t_2 on the surface, respectively. Then, for TE polarization, using the generalized Fock theory [7], [8], one obtains

$$\vec{H}(Q_0) = \vec{H}_i(Q_1)e^{-j\beta t_1} g(\xi_1) + \vec{H}_i(Q_2)e^{-j\beta t_2} g(\xi_2) \tag{19}$$

where

$$\xi_{1,2} = \int_{Q_{1,2}}^{Q_0} \frac{m(t')}{\rho_g(t')} dt' \tag{20}$$

$$m(t') = [\beta\rho_g(t')/2]^{1/3} \tag{21}$$

$$t_{1,2} = \int_{Q_{1,2}}^{Q_0} dt' \tag{22}$$

$$g(\xi) = e^{\frac{-j\xi^3}{3}} \frac{1}{\sqrt{\pi}} \int_c e^{-j\xi t} \frac{dt}{w_1'(t)} \tag{23}$$

$\rho_g(t')$ is the radius of curvature at t' and the Airy function $w_1(t)$ and the contour "c" are defined in [4].

Once the magnetic field is found, the current on the surface is determined from

$$\vec{J} = \hat{n} \times \vec{H} . \tag{24}$$

For the specific case of a circular cylinder excited by a TE-plane wave, the initial estimate for the shadow-side current, J_E^s, is given by

$$J_E^s = \hat{n} \times \vec{H} \tag{25}$$

with $\vec{H}$ being given by

$$\vec{H} = \hat{z}H_o\{e^{-j\beta t_1}g(\xi_1) + e^{-j\beta t_2}g(\xi_2)\} \qquad (26)$$

where

$$\xi_1 = \left(\frac{\beta a}{2}\right)^{1/3} \frac{t_1}{a}$$

$$\xi_2 = \left(\frac{\beta a}{2}\right)^{1/3} \frac{t_2}{a}$$

a = radius of circular cylinder. (27)

Using Equations (25) to (27), Fock current in the shadow side has been computed for a circular cylinder of radius 3.2λ and is shown in Figure 6. Notice that expressions given here are valid only for TE polarization. Similar expressions can be easily obtained for TM polarization.

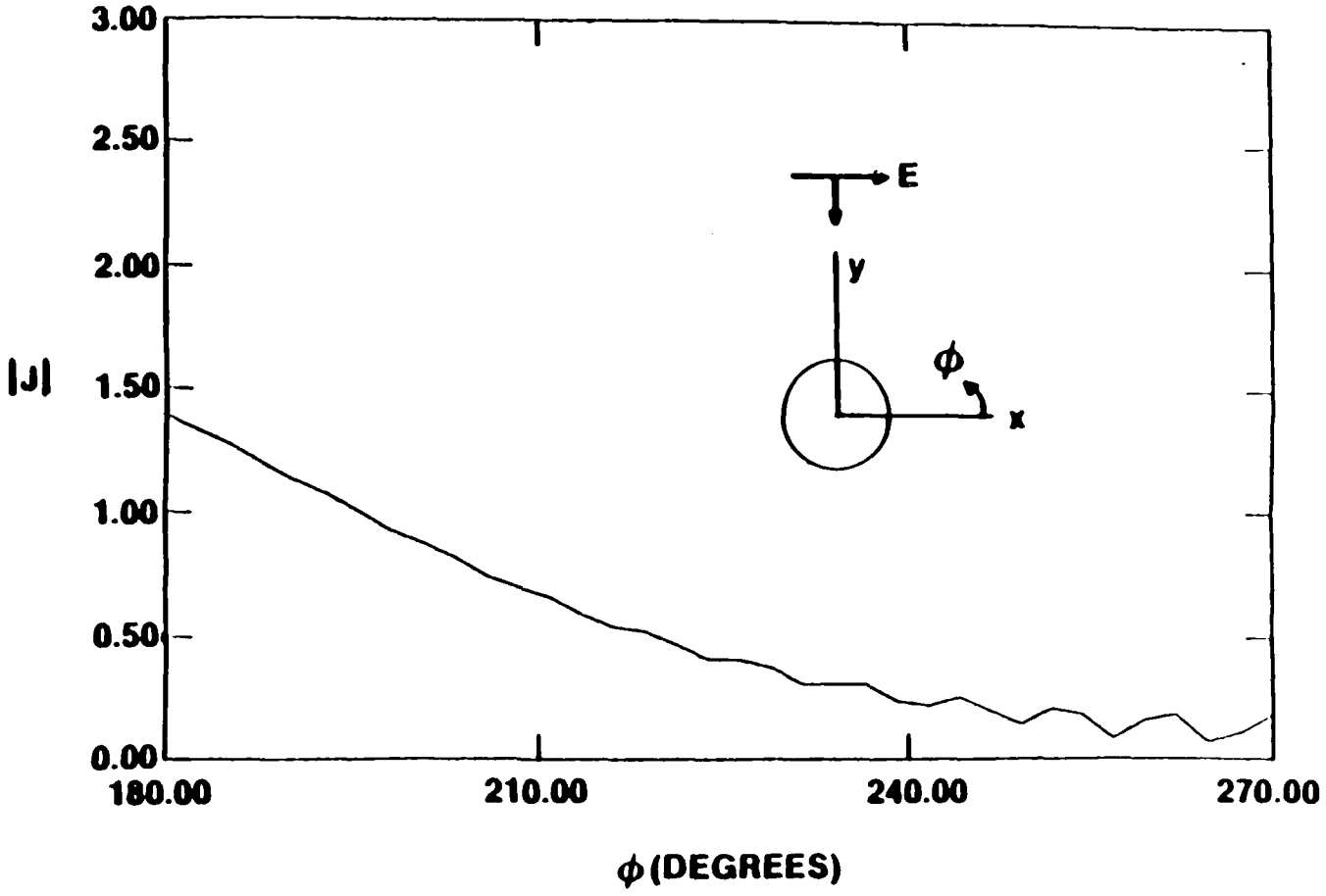

Figure 6. Shadow side Fock current on a circular cylinder.
Radius 3.2λ, $\phi_i = 90^0$
_____ Method of Moments
- - - - HIM

SECTION 4
NUMERICAL EXAMPLES

In this section, we illustrate the technique described in earlier sections. We deal with scatterers with surface discontinuities as well as smooth surfaces. Thus, 1) scatterers with edges are exemplified by a square cylinder; 2) scatterers with smooth surfaces are exemplified by circular and elliptical cylinders; and 3) scatterers with a smooth surface joined to an edge are exemplified by the ogival cylinder.

Before the theory presented in earlier sections can be used to compute the induced currents, some numerical aspects must be considered. For scatterers with edges, special attention must be paid to evaluating the integrals for current very close to the edge. This analysis has been dealt with elsewhere [2], [3] and will not be repeated here. For scatterers with smooth surfaces, it is necessary to evaluate integrals wherein the integration and observation points may coincide. In such cases, the Green's function becomes singular and one must consider the principle value of the integral. For two-dimensional geometries, however, it can be shown [2], [3] that the integrands have a finite limit.

The following results will be for zeroth order, first-order and second-order currents. It is necessary to understand what this means. The zeroth-order currents are defined by Eqs. (10) and (11). The zeroth-order currents are themselves obtained by iteration, say ten iterations. Once a converged zeroth-order current has been obtained according to the criterion of Eq. (16), the zeroth-order current, is used in Eqs. (12) and (13) to obtain the first-order currents via iteration, etc.

4.1 SQUARE CYLINDER

Two examples are presented here. In both cases, the size of the cylinder is the same, viz, $w = 3.7\lambda$. However, the angles of incidence, ϕ_i, are different. The case, $\phi_i = 115^0$, has been

dealt with in an earlier report [3]. We study the same case here using our hybrid-iterative method (HIM). It was necessary in [3] to compute four orders of correction currents to obtain a sufficiently accurate result. With the HIM, zeroth order currents themselves give a sufficiently accurate solution. We also present the first-order currents for comparison. Figures 7 to 11 show the results for $w = 3.7\lambda$ and $\phi_i = 115^0$.

We also consider the case when $\phi_i = 95^0$. Note that in this case, Face 2 of the square cylinder is almost, but not quite, in the visible region. As can be seen from the final result, the current on this face is quite appreciable and may not be neglected initially as was done in the iterative technique [2], [3]. Figures 12 to 16 show results corresponding to this case. In this more demanding case it was necessary to compute up to the second-order currents.

4.2 SCATTERERS WITH SMOOTH SURFACE

In [2], Kaye, Murthy and Thiele used the iterative method (IM) to compute the surface currents on a circular cylinder of radius 3.2λ. These computations include the first-order correction current and are characterized by a ripple. For the same cylinder, we computed induced currents using the HIM. These results are presented in Figures 17 to 19. Note that there is no ripple and that the agreement between our results and the exact eigenfunction solution is excellent. Furthermore, we needed to compute only up to the zeroth-order currents. After zeroth iteration, HIM yielded an error of ε_o (HIM) = 0.0018. The VAX CPU time taken is 2 minutes and 18 seconds. For the same case, with iteration method, ε_o (IM) = 0.054 and ε_1 (IM) = 0.047. Thus, even after the first-order calculation, the average error for IM is significantly larger than that for HIM. The CPU time required for IM up to first-order calculations is three minutes and 45 seconds. All computations were carried out on a VAX 11/780.

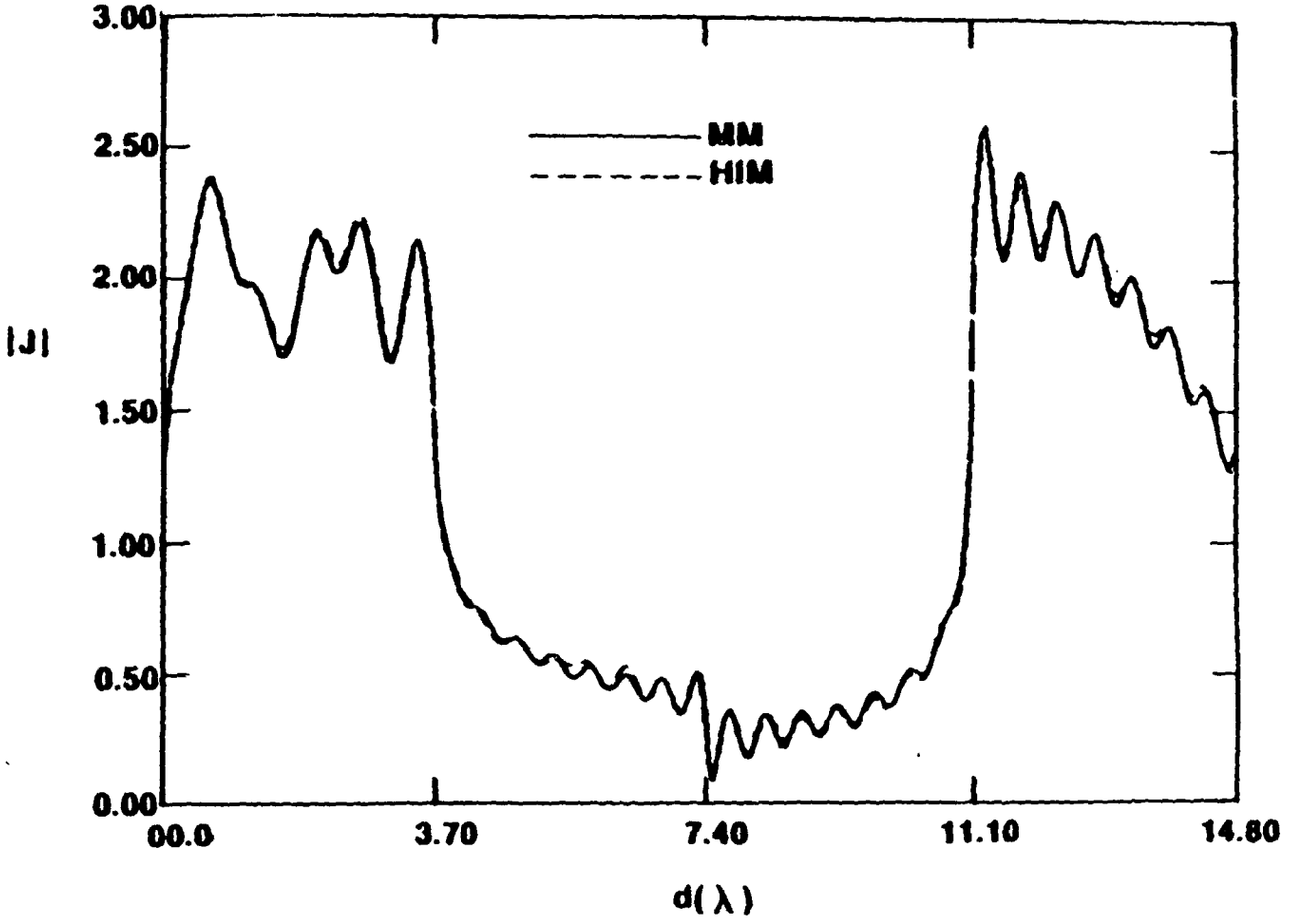

Figure 7. Magnitude of current on a square clyinder. Order = 0, $w = 3.7\lambda$, $\phi_i = 115^0$

_____ Method of Moments

- - - - HIM

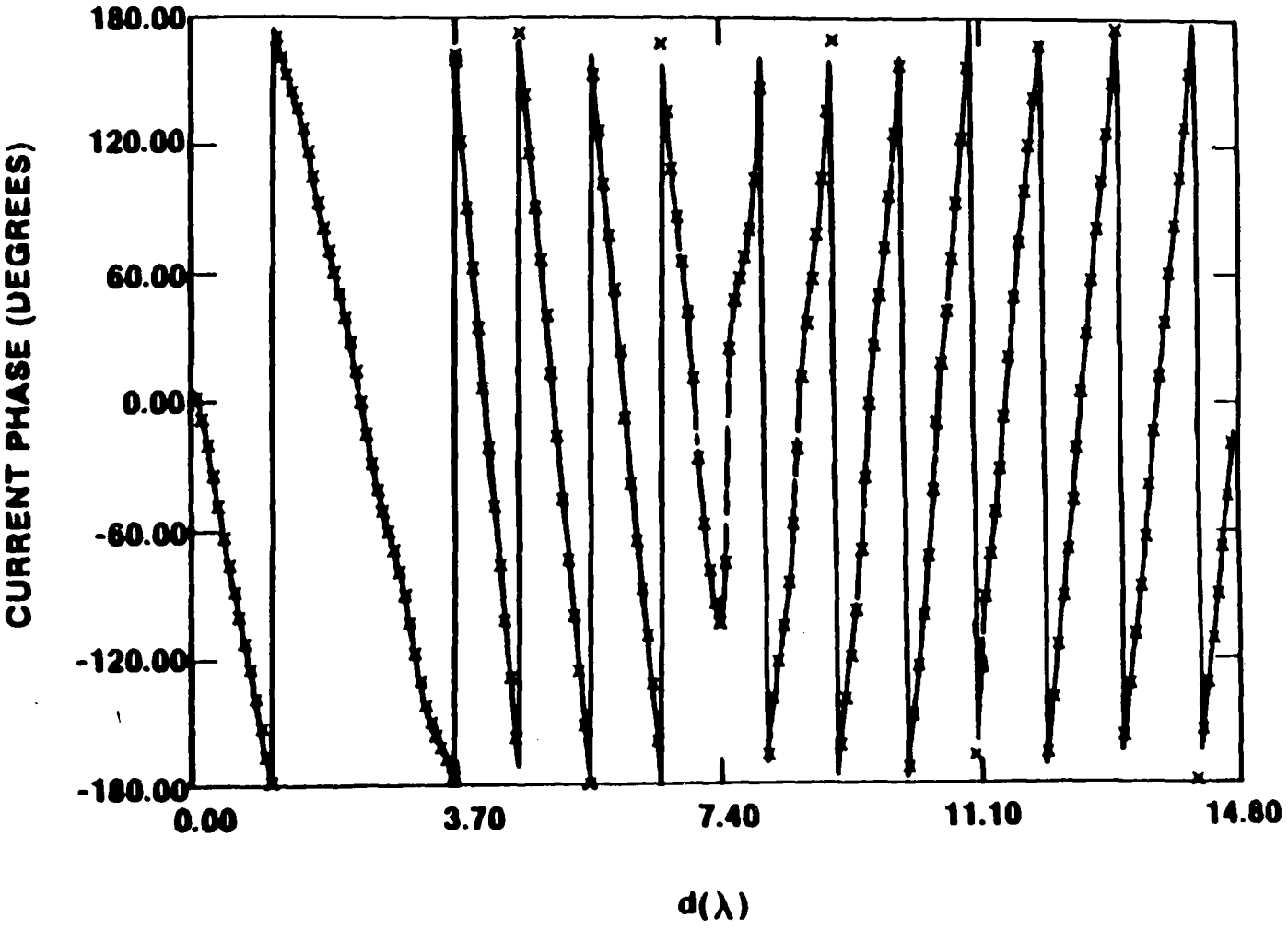

Figure 8. Phase of current on a square cylinder. Order = 0, $w = 3.7\lambda$, $\phi_i = 115^0$

_____ Method of Moments

x x x x IIM

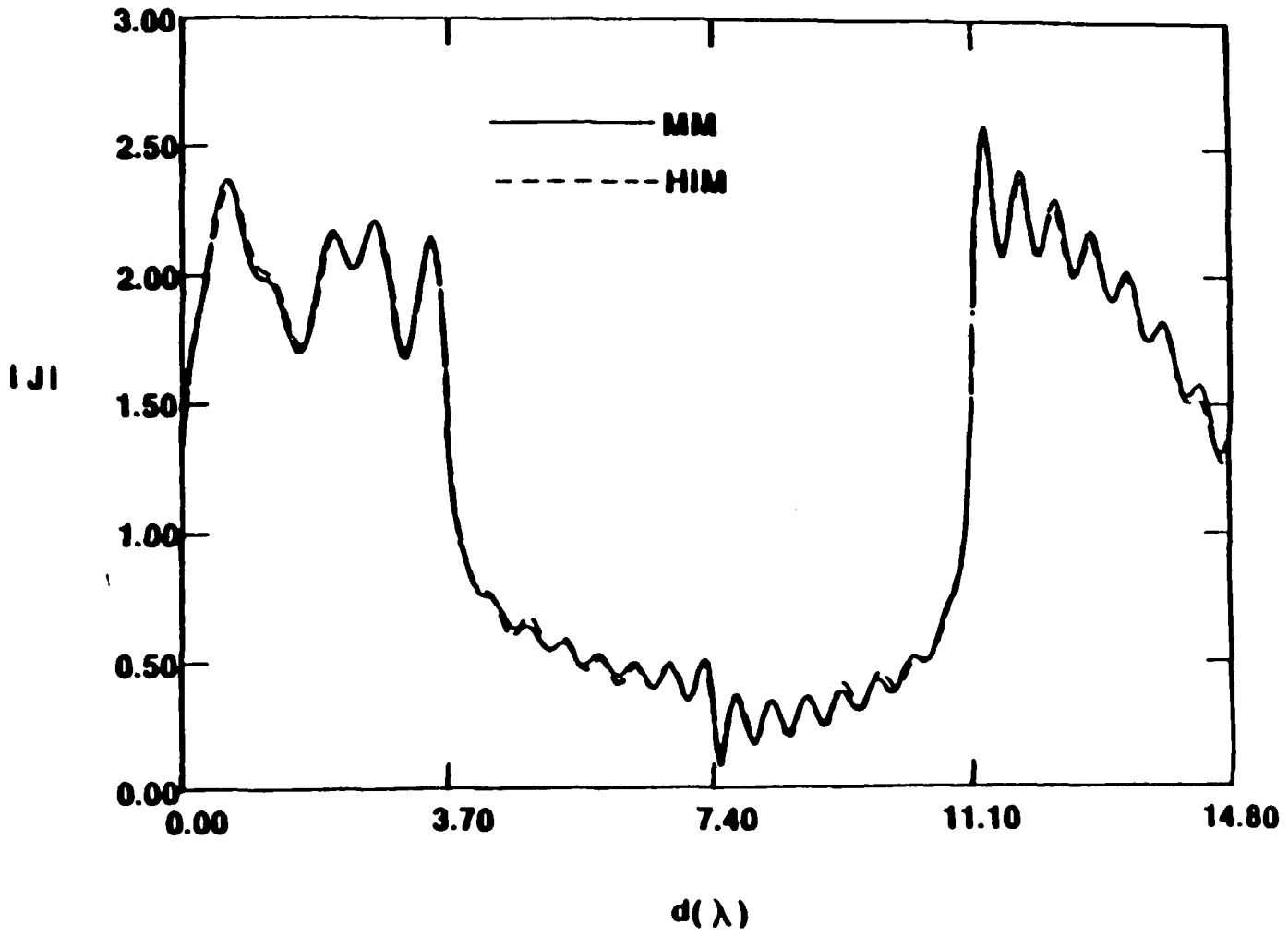

Figure 9. Magnitude of current on a square cylinder. Order = 1, $w = 3.7\lambda$, $\phi_i = 115^0$

_____ Method of Moments

- - - - HIM

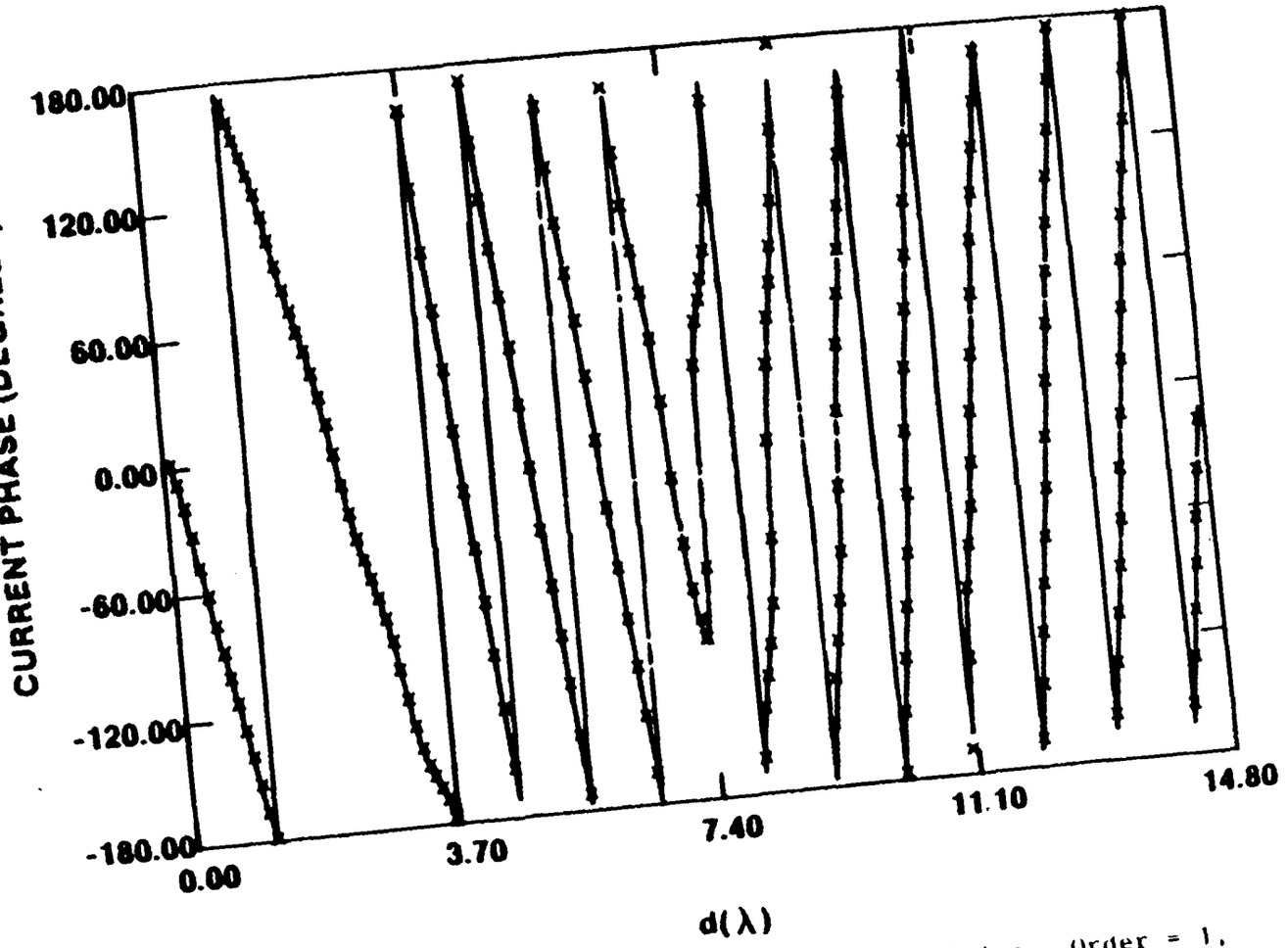

Figure 10. Phase of current on a square cylinder. Order = 1, $w = 3.7\lambda$, $\phi_i = 115^0$

———— Method of Moments

x x x x HIM

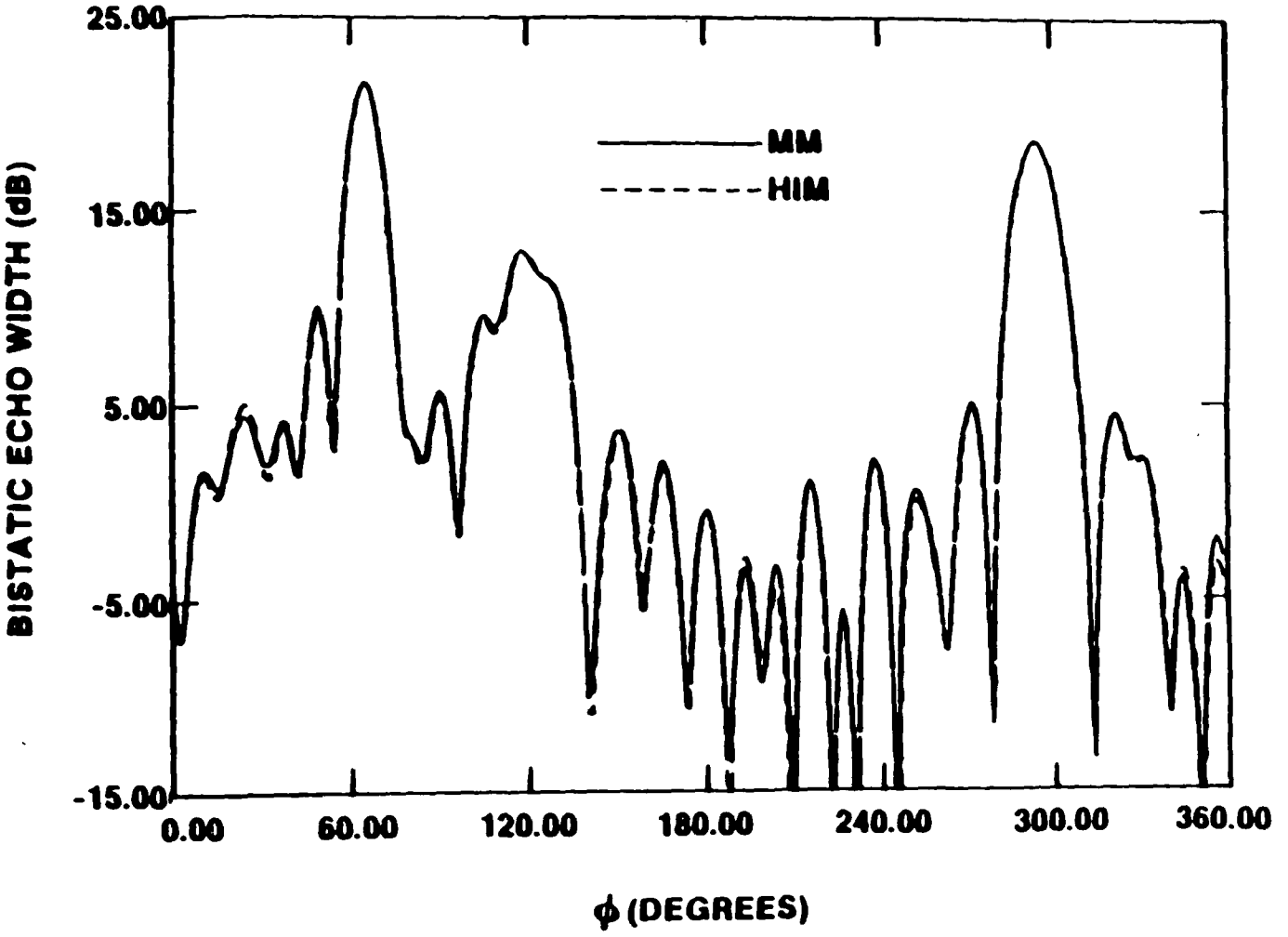

Figure 11. Bistatic echo width of a square cylinder. Order = 1, $w = 3.7\lambda$, $\varphi_1 = 115^0$

———— Method of Moments

- - - - HIM

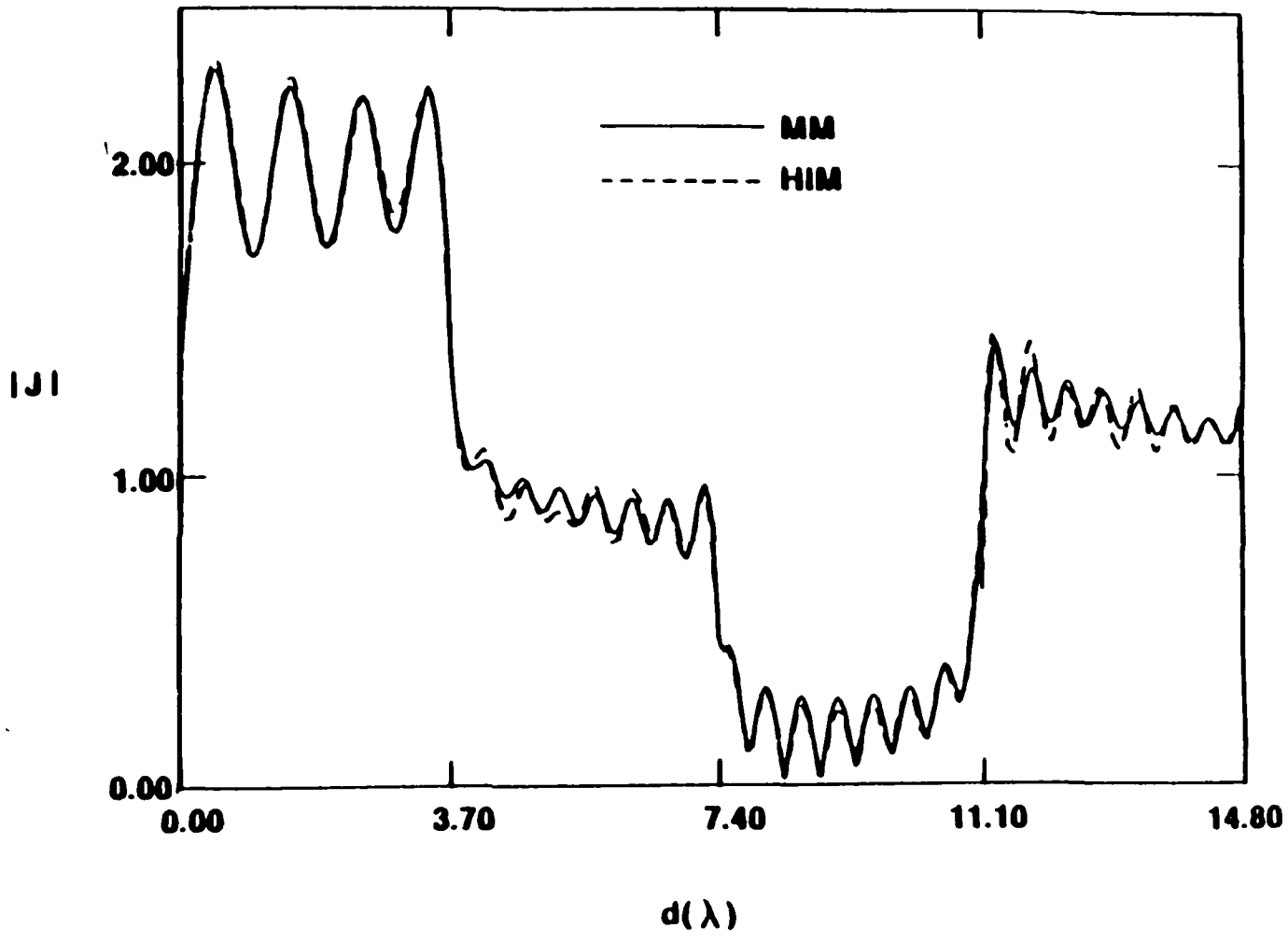

Figure 12. Magnitude of current on a square cylinder.
Order = 0, w = 3.7λ, $\phi_i = 95^0$
_____ Method of Moments
- - - - HIM

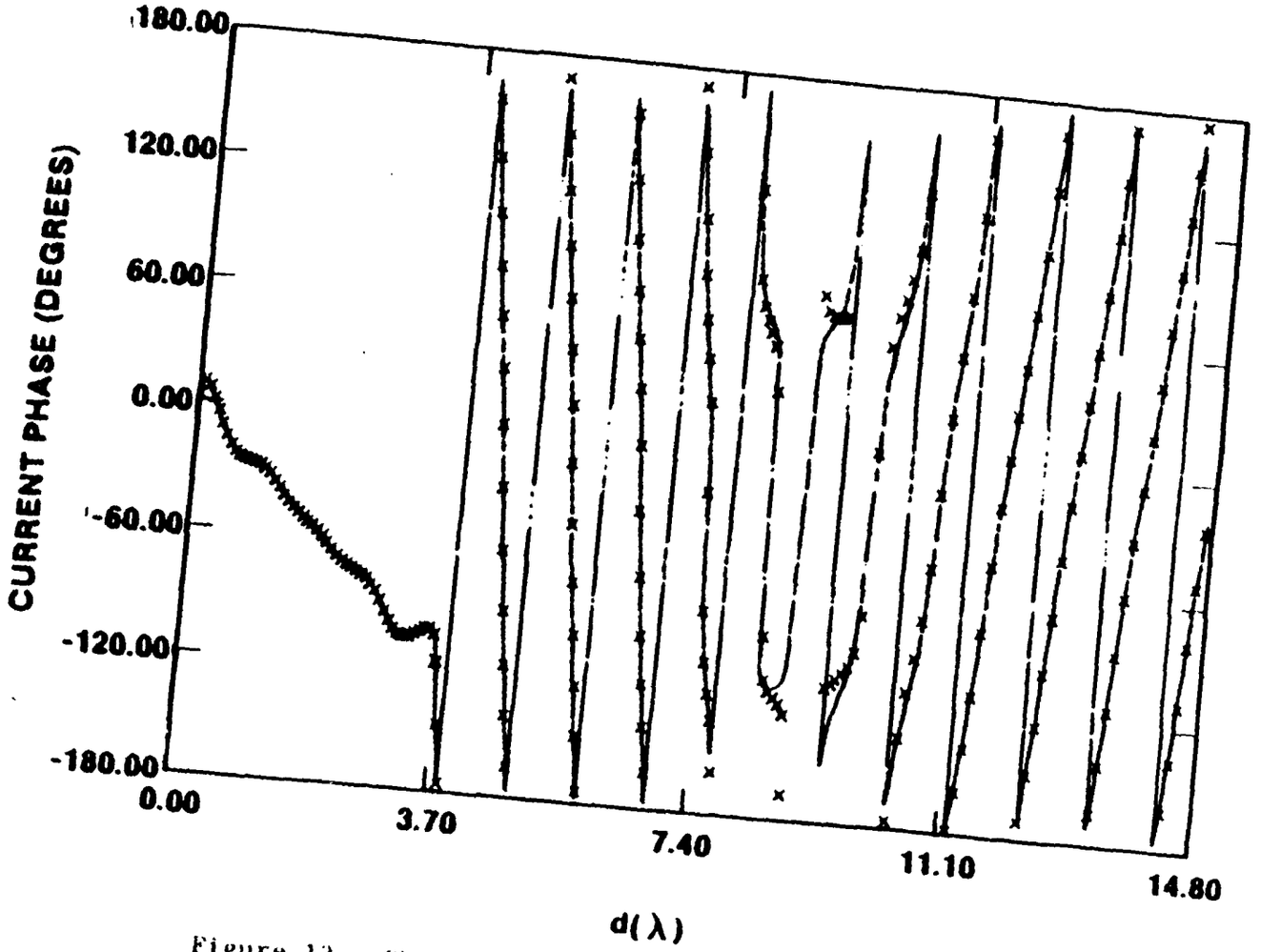

Figure 13. Phase of current on square cylinder. Order = 0, $w = 3.7\lambda$, $\phi_i = 95^0$

———— Method of Moments

x x x x HIM

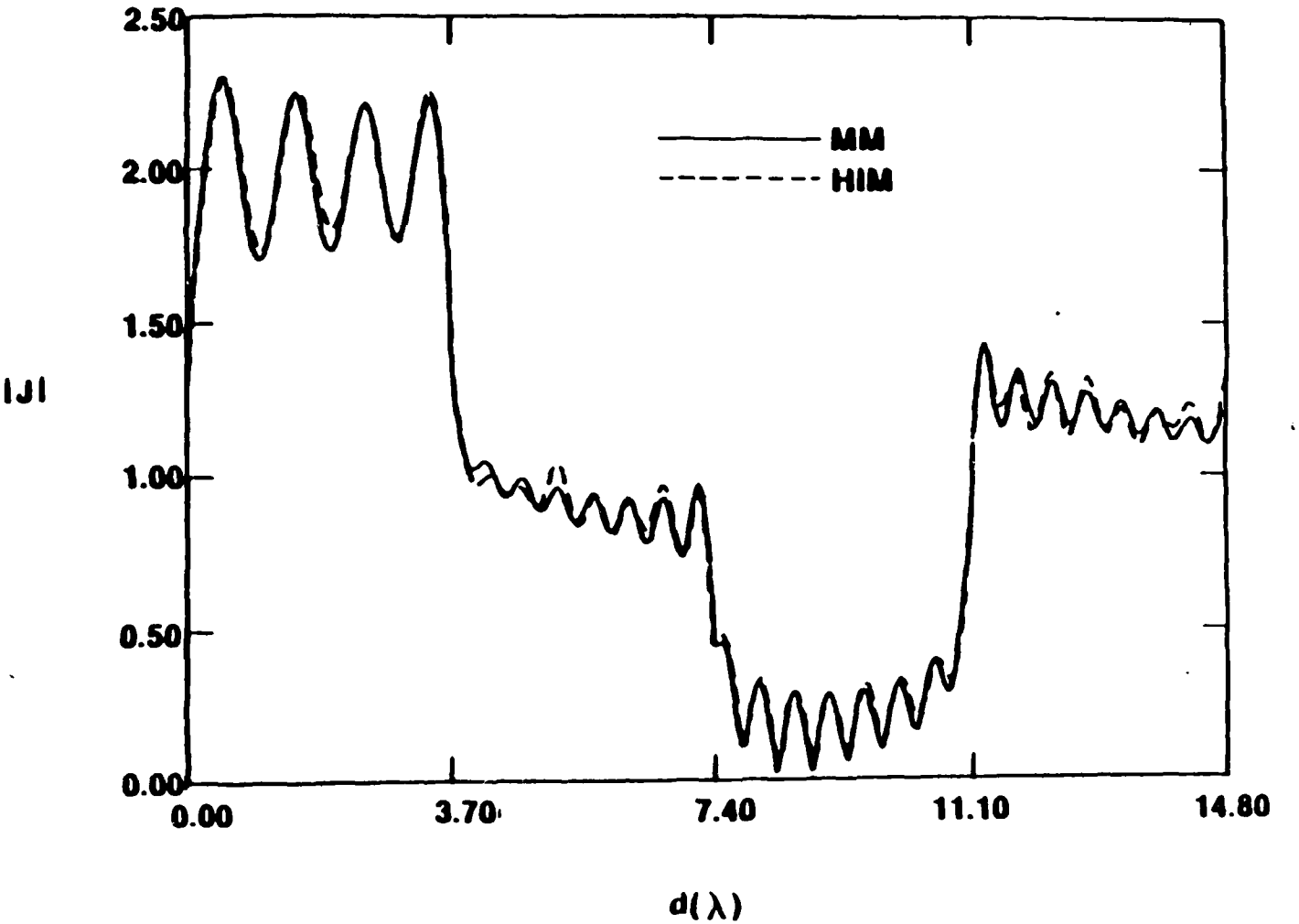

Figure 14. Magnitude of current on a square cylinder.
Order = 2, ew = 3.7λ, $\psi_i = 95^0$
_____ Method of Moments
- - - - HIM

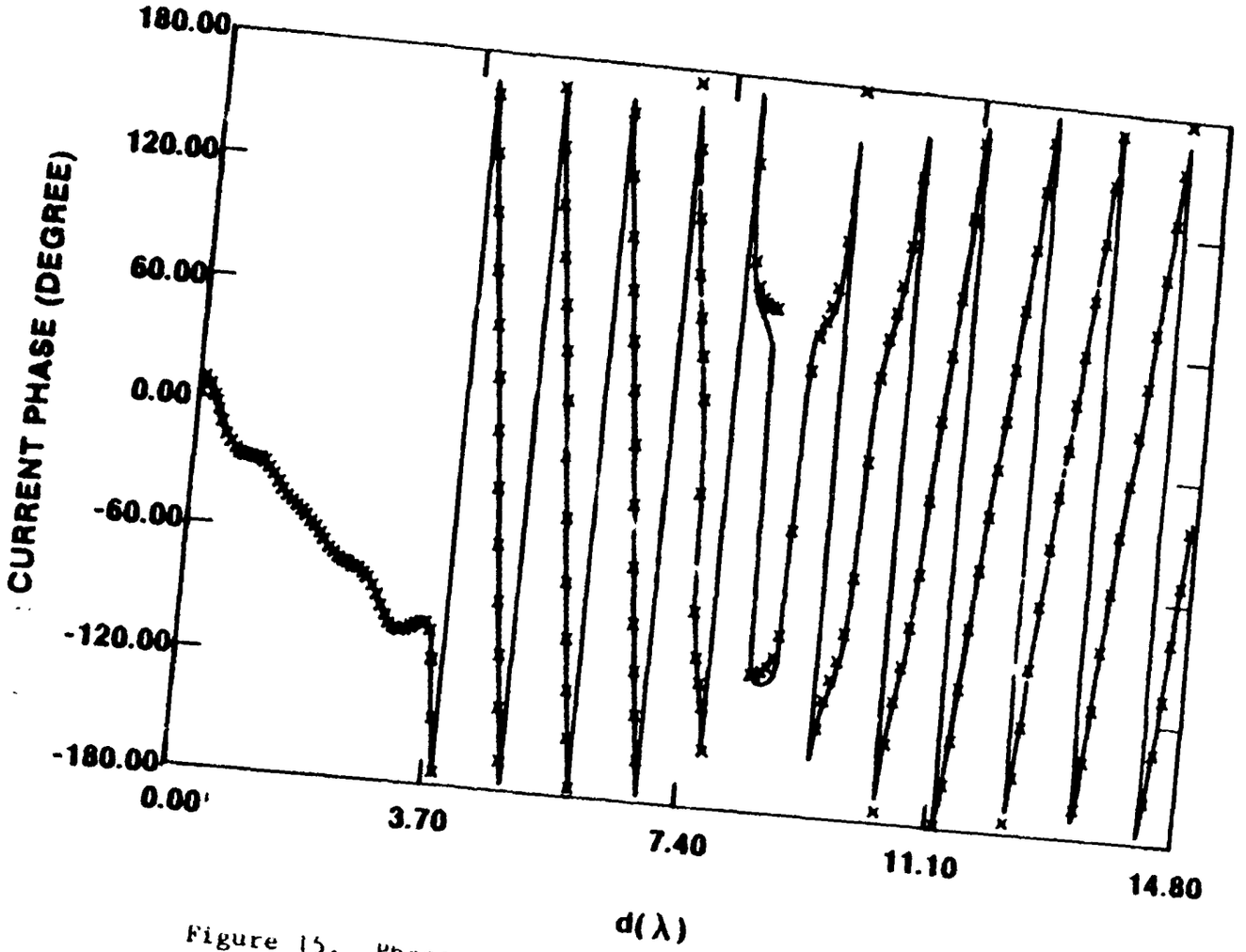

Figure 15. Phase of current on a square cylinder. Order = 2, $w = 3.7\lambda$, $\phi_i = 95^0$

———— Method of Moments

x x x x HIM

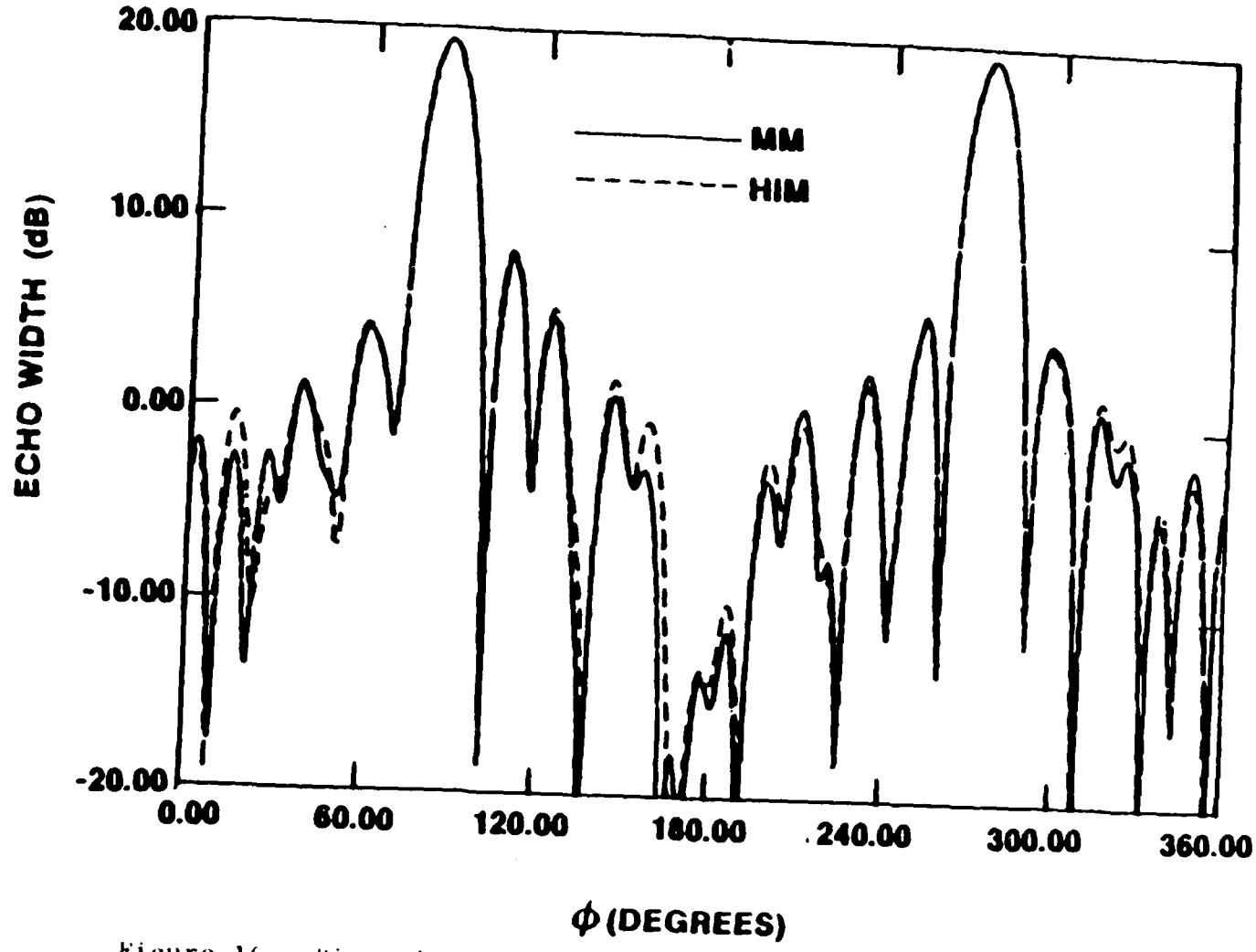

Figure 16. Bistatic echo width of a square cylinder. Order = 2, $w = 3.7\lambda$, $\phi_i = 95^0$

_____ Method of Moments

- - - - HIM

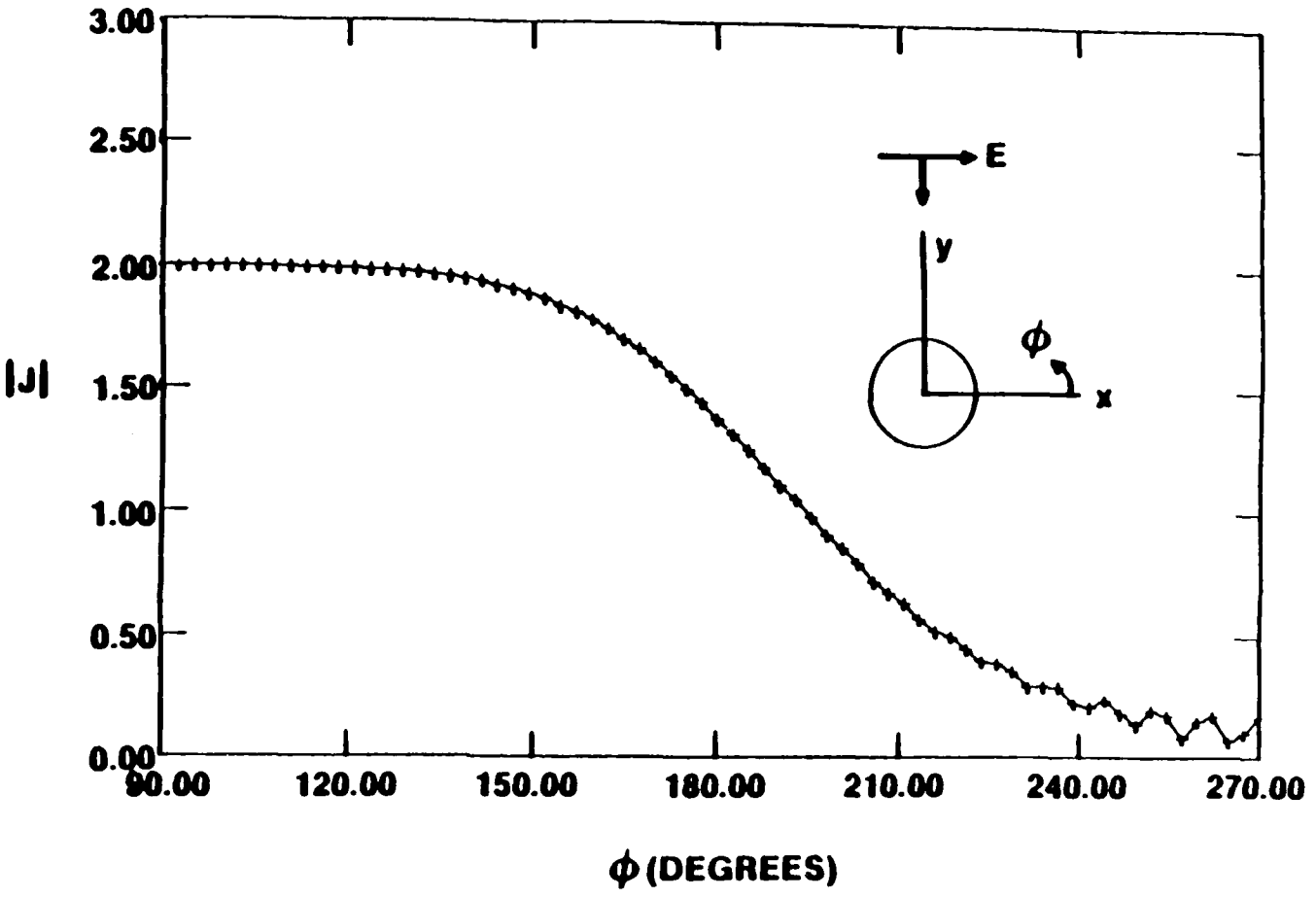

Figure 17. Magnitude of current on a circular cylinder. Order = 0, Radius = 3.2λ, $\phi_i = 90^0$

_____ Method of Moments

x x x x HIM

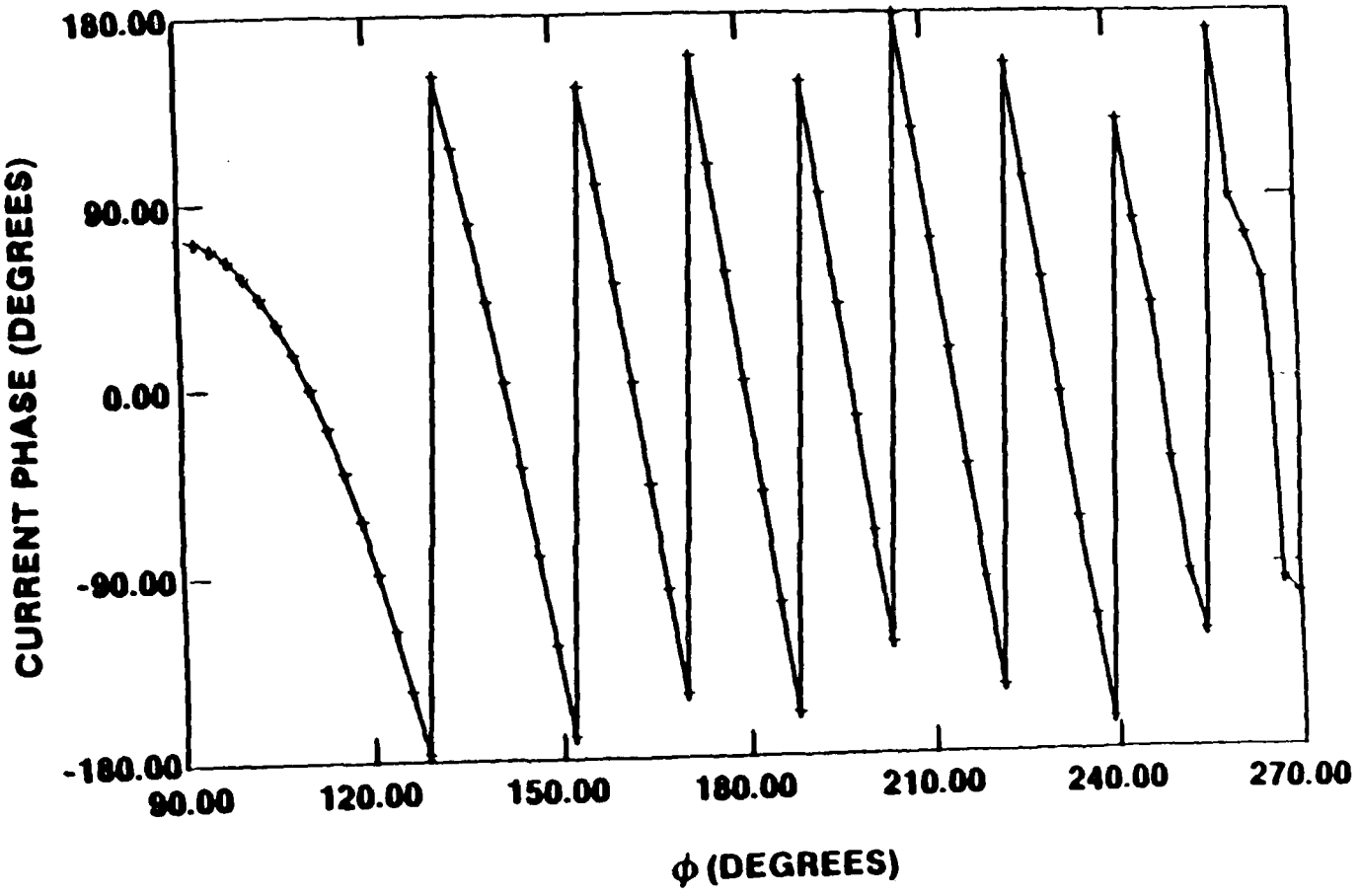

Figure 18. Phase of current on a circular cylinder. Order = 0, Radius = 3.2λ, $\varphi_i = 90^0$

_____ Exact Solution

x x x x MM

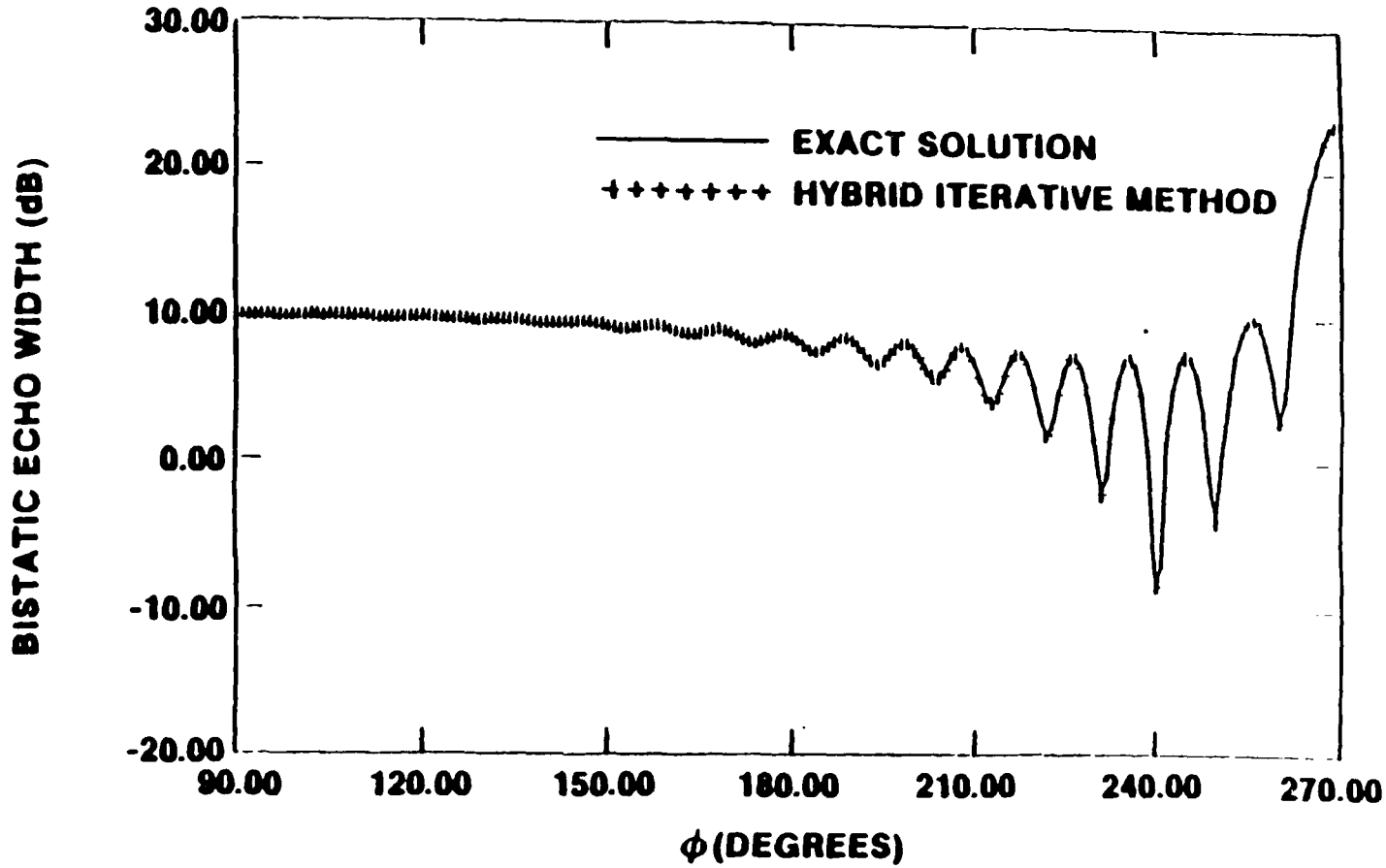

Figure 19. Bistatic echo width of a circular cylinder.
Order = 0, Radius 3.2 λ, $\phi_i = 90^0$

In order to demonstrate that our technique works well for "small" bodies, we also considered a 0.2λ radius circular cylinder in [9]. We computed both zeroth-order and first-order currents with excellent agreement between our results and the exact results obtained using the eigenfunction solution.

The computer code we have written is general and may be used to compute the induced currents on scatterers with an arbitrary convex cross-section. To demonstrate this generality, we have also considered an elliptic cylinder as shown in Figure 20 with semi-major and semi-minor axes being 1.5λ and 1.0λ, respectively. Our results are compared with those of the method of moments (MM). A result is shown in Figure 21. Note the excellent agreement between the results obtained with the MM and and with the hybrid-iterative technique.

4.3 SCATTERERS WITH A SMOOTH SURFACE JOINED TO AN EDGE

The ogival cylinder is an example of a smooth surface joined to an edge. To illustrate the application of HIM to the ogival cylinder, we will consider a 3λ long (edge-to-edge) ogival cylinder with an 80^0 interior "wedge" angle at each edge. Figure 22 shows the current on one side of the ogival cylinder for a plane wave incident at 90^0. The current is of zeroth order and the agreement is seen to be excellent. The traveling wave, for which the ogive is well-known, would be predicted by the current in Figure 22. Figure 23 shows the ogival cylinder illuminated broadside (i.e., at 0^0). This is a more difficult case than with 90^0 (edge on) incidence. Thus, second-order currents are required to obtain excellent agreement.

4.4 VERY LARGE SCATTERERS

For the purpose of adapting the HIM to treat scatterers that are electrically large, the surface current is considered to consist of two components: the physical optics current and the

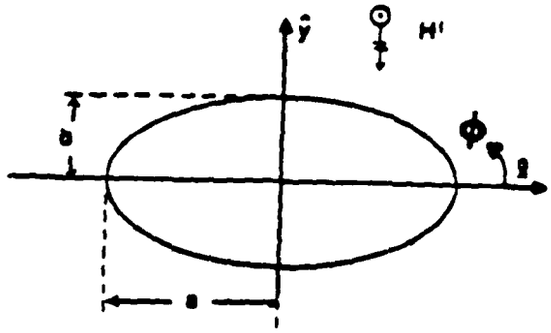

Figure 20. Geometry for an elliptic cylinder with semi-major axis "a" and semi-minor "b". $\varphi_i = 90^0$

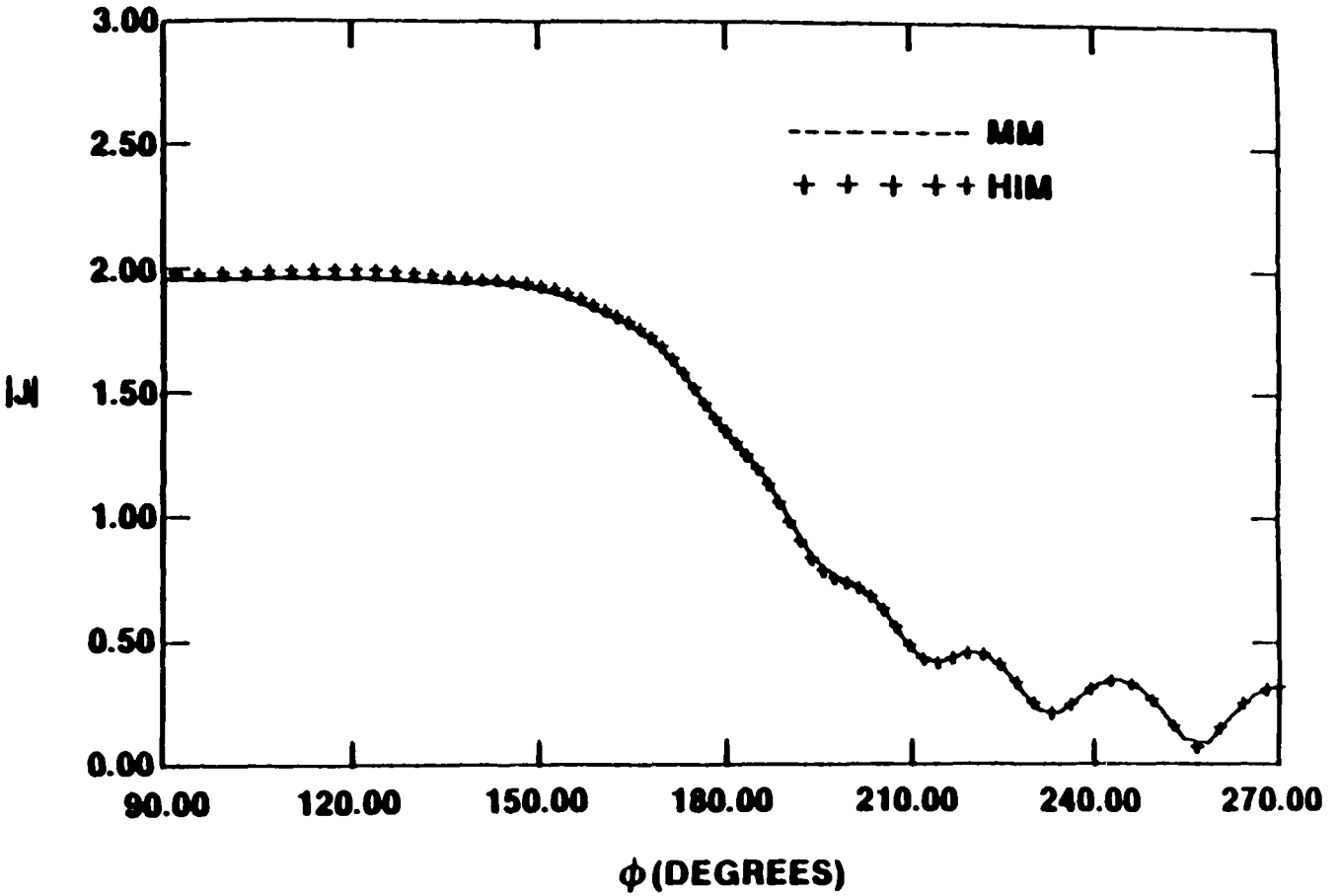

Figure 21. Magnitude of current on an elliptic cylinder. Order = 0, a = 1.5λ, b = 1.0λ, $\phi_i = 90^0$

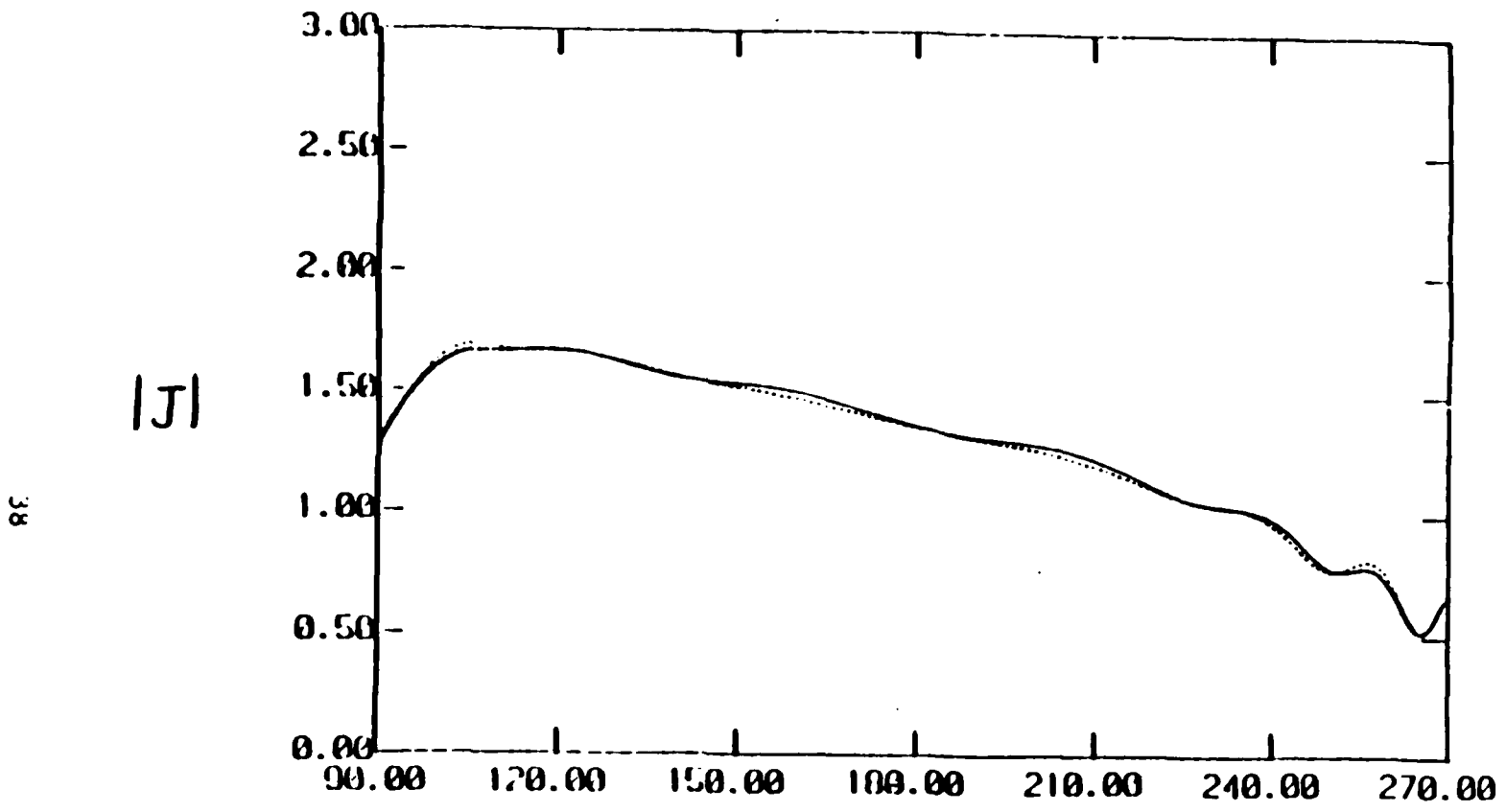

Figure 22. Ogival cylinder results for a 3λ long 80° ogive with edge-on incidence. Current is zeroth order only. Excellent agreement between HIM and MM.

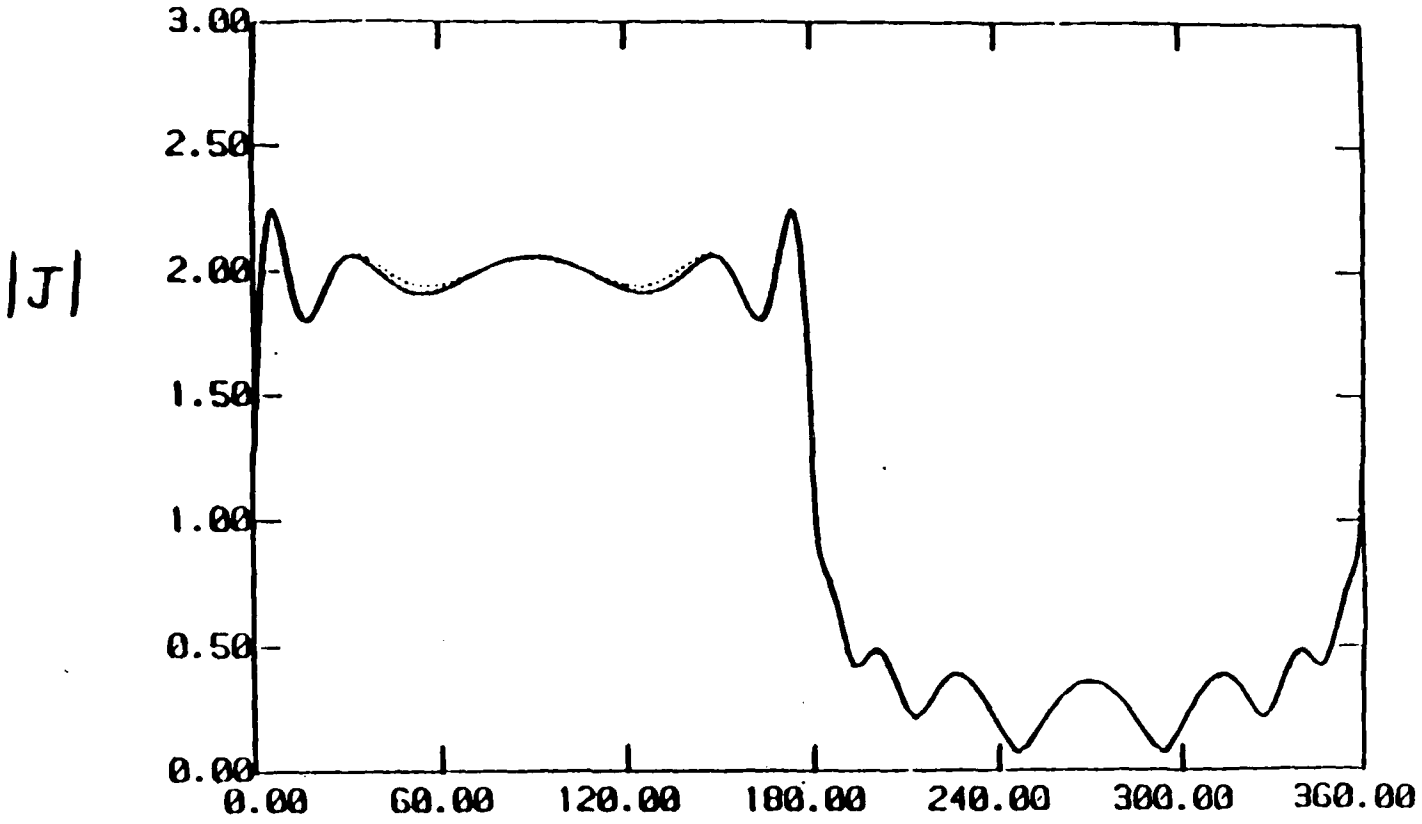

Figure 23. Same as Figure 22 except incidence is "broadside" and current is second order since this is a more difficult case than edge-on incidence. Note that this is an example of a curved surface joined to an edge.

nonuniform current. The physical optics current is readily determined. Since the nonuniform current is induced by the diffracted field at the surface, it decays relatively quickly from the point of diffraction. Thus, though the scatterer is large, the region over which the nonuniform current is unknown is relatively small. This is the basic principle behind the reformulation of HIM for large bodies. Additionally, the integrals involved are in a form suitable for evaluation by the stationary-phase method; this form is used wherever feasible. Thus, numerical integration is used to the least extent necessary. We give the specific formulation for a circular cylinder in [10], though the method itself is more general than presented there.

Figures 24 and 25 illustrate the foregoing principles by presenting a comparison of the current between the exact eigenfunction solutions and the calculated results obtained by use of this reformulated scheme for the circular cylinder with radii equal to 25 and 80 wavelengths. The stationary-phase evaluation, in the result shown, only includes the endpoint contribution because the stationary points are outside the integration path. The CPU time required to run the result of this 25-wavelength-radius cylinder on a VAX 11/780 computer is approximately eight minutes; while the CPU time required for a cylinder with an 80-wavelength radius is approximately 40 minutes.

The large body formulation for HIM is adaptable for use on a super computer like th Cray X-MP. On May 19, 20, and 21, 1986, we ran our program for the large cylinder on the Cray X-MP at the Cray facility in Minneapolis under the sponsorship of Cray Research. Some rewrite of our program was necessary to permit the compiler to vectorize the code. The results are presented in the table which follows. Note that for the 80λ cylinder the VAX time was about 2,400 seconds and that on the Cray X-MP, after rewrite and vectorization, the CPU time was but 6.17 seconds.

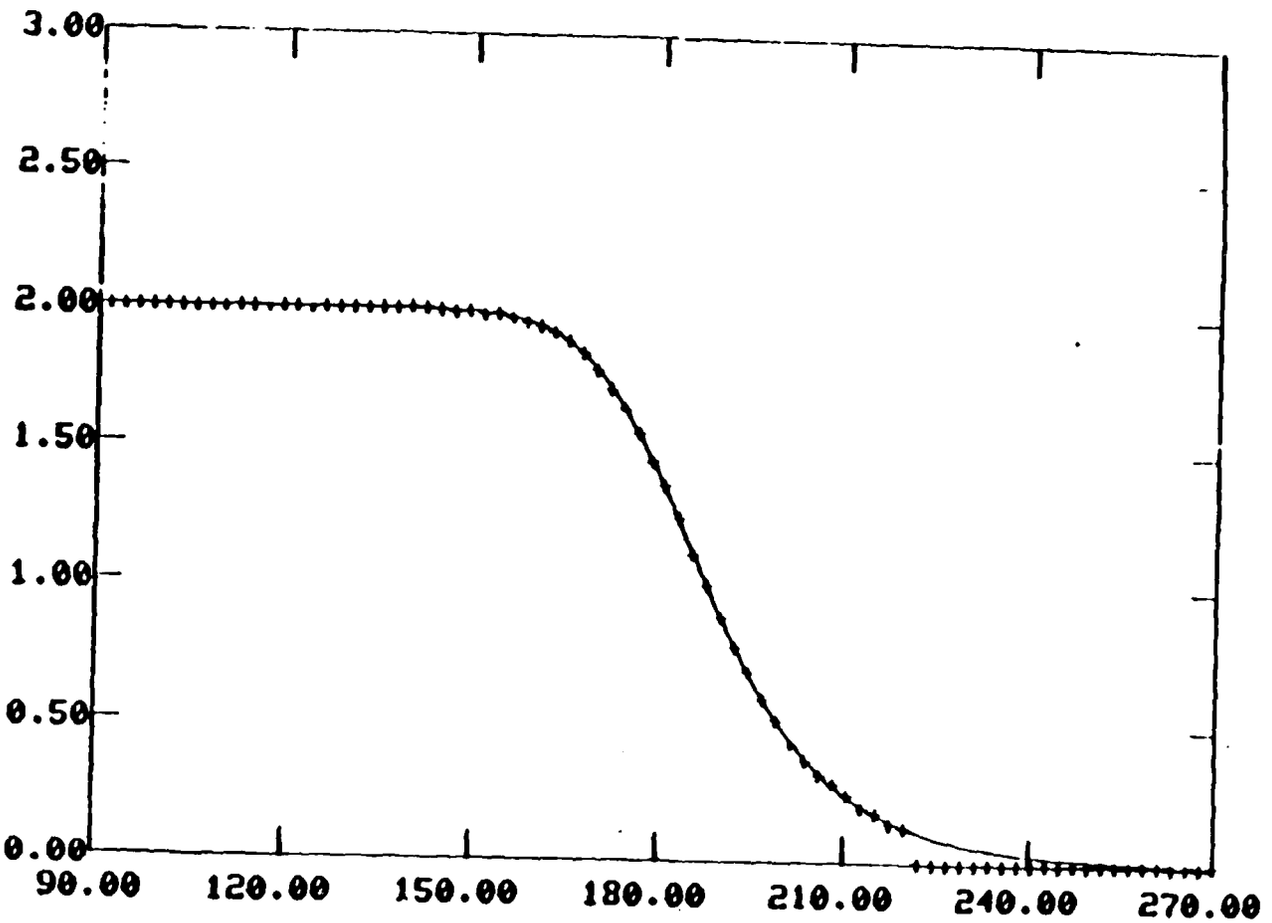

Figure 24. Large circular cylinder example with a = 25λ.
See chart for computer times.

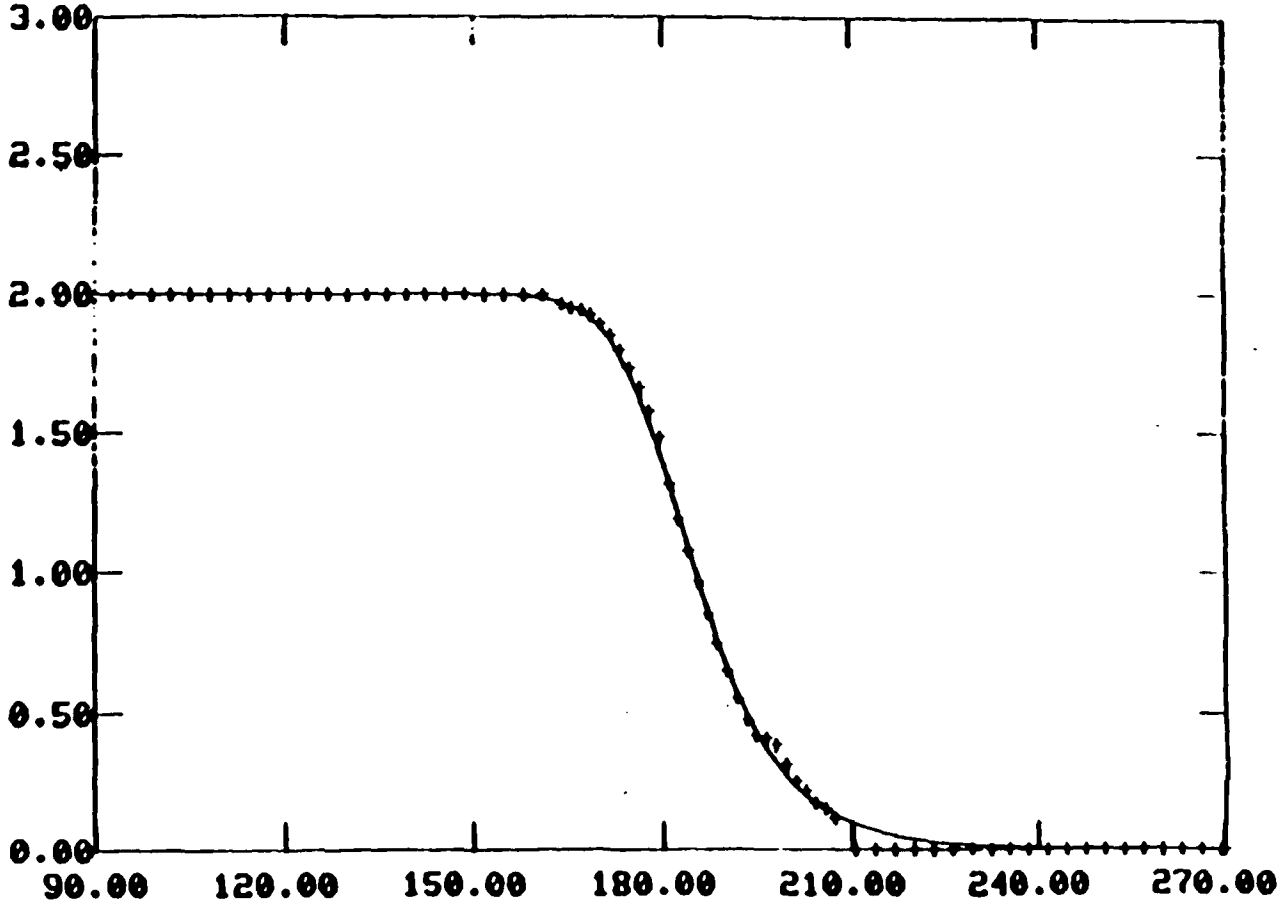

Figure 25. Large circular cylinder example with a = 80λ. See chart for computer times.

RCS

COMPUTER TIMES FOR LARGE CIRCULAR CYLINDERS

RADIUS (λ)	~C(λ)	VAX*	CRAY X-MP*	RATIO
10	63	60	0.37	162
25	157	480		
80	500	2,400	6.17	389
120	750		10.5	
160	1,000		15.3	
200	1,250		20.5	
240	1,500		26.0	
300	1,880		34.8	
400	2,500		50.6	
440	2,760		56.9	

* TIME IN SECONDS

While this ratio of 389 to 1 was not the largest ratio the Cray Applications Group had ever seen, it was in the class of very large ratios that one can achieve in going from a VAX to a Cray. They viewed a ratio of 100 or over as very good.

Note that the small CPU times indicate that the HIM could be used as an interactive design tool. For example, one could design any wing profile and any radar frequency interactively using this HIM approach.

Note that we used here the (classical) circular cylinder shape because we have an exact solution against which to compare. Cylinders of other cross section shapes would have similar running times.

4.5 PERFECTLY CONDUCTING CUBE

Figure 26 shows the geometry for a perfectly conducting cube. Figures 27-32 show the H-plane and E-plane bistatic scattering pattern for cubes that are 0.75λ, 1.5λ and 3.0λ on a side, respectively. In all cases, agreement with experimental data furnished by RADC/Hanscom is seen to be quite good. Also included are figures 33-36, which describes the surface current densities on the cube faces. Figure 33 describes the magnitude of the z-component of the initial current on the side face, while figure 34 shows that same current aften imposition of the M.F.I.E. It is seen that the composite effects of slope diffraction and vertex diffraction, previously ignored, have been introduced. Figures 35 and 36 describe current components initially assumed to be zero. After imposing the M.F.I.E., it is seen that a much better, non-zero approximation results.

4.6 TM CASE FOR SQUARE CYLINDER

Our results in Section 4.1 for the square cylinder were for the TE case. Clearly, to do the cube in Section 4.5 it was necessary to be able to calculate TM currents as well as TE

currents. Here, in this section, we will briefly present some results for TM currents on a square cylinder.

Figure 37 shows the magnitude of the fourth-order current on a square cylinder 3.193λ on a side. The incidence angle is $\phi_i = 135^0$ (see Figure 4). Figure 38 shows the phase. Figures 39 and 40 show similar results except that the incidence angle is 120^0.

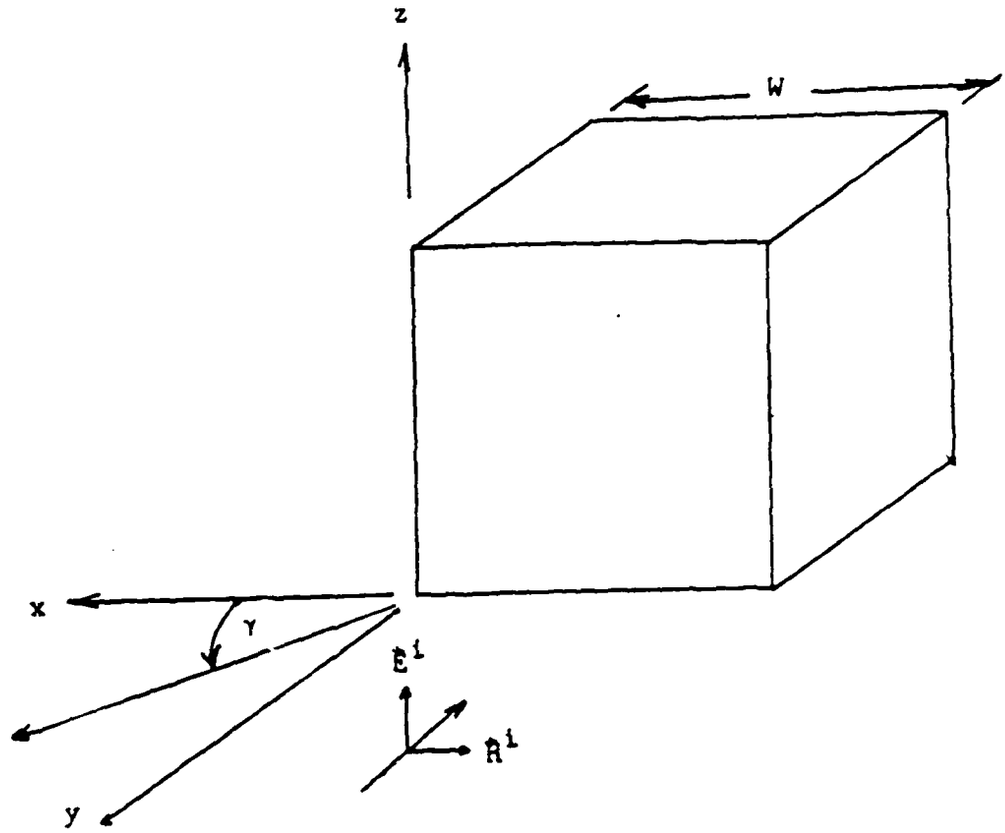

Figure 26. Note: $\gamma = 90^0$ Backscatter
$\gamma = 270^0$ Forward scatter.

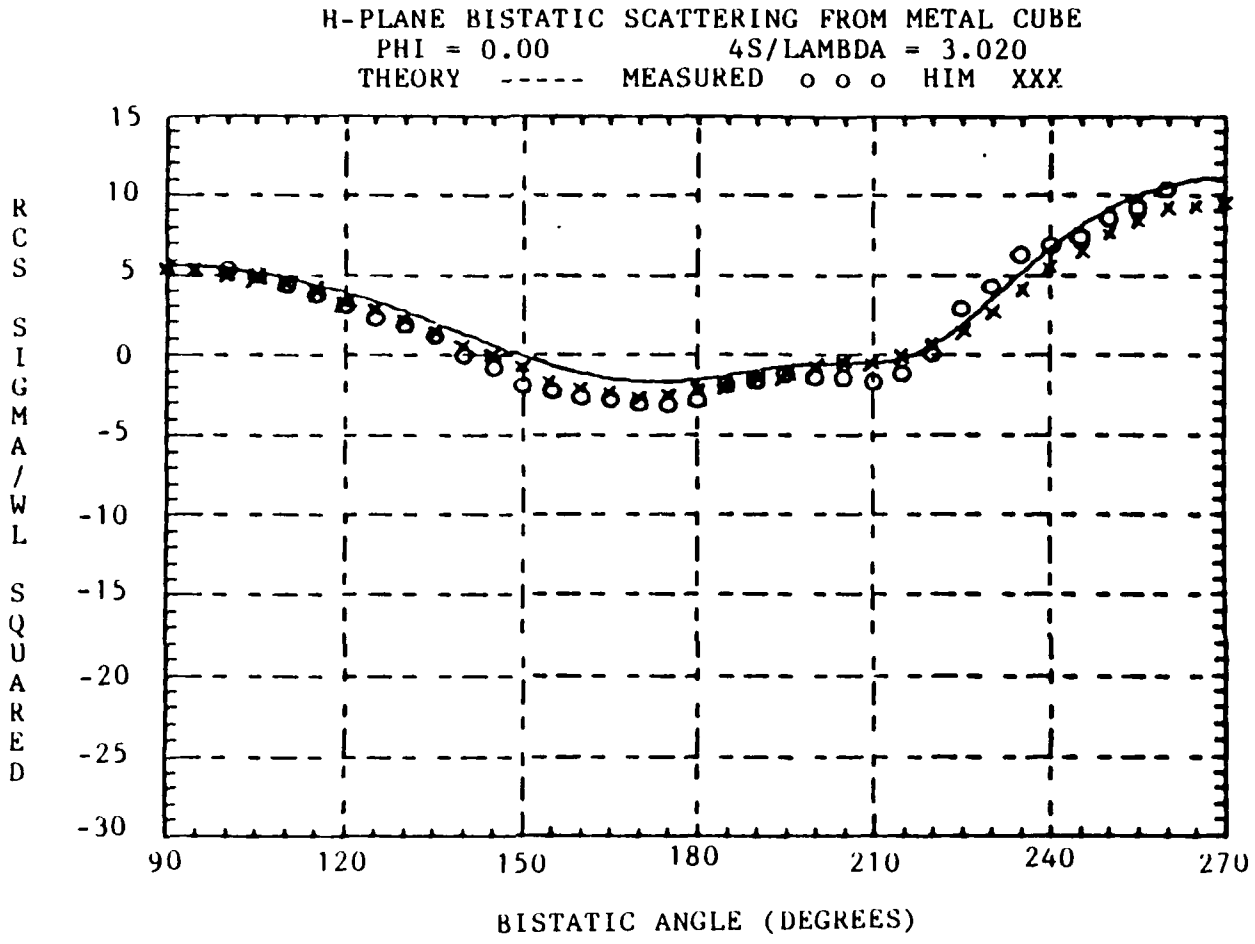

Figure 27. H-plane bistatic scattering from a metal cube 0.75λ on a side.

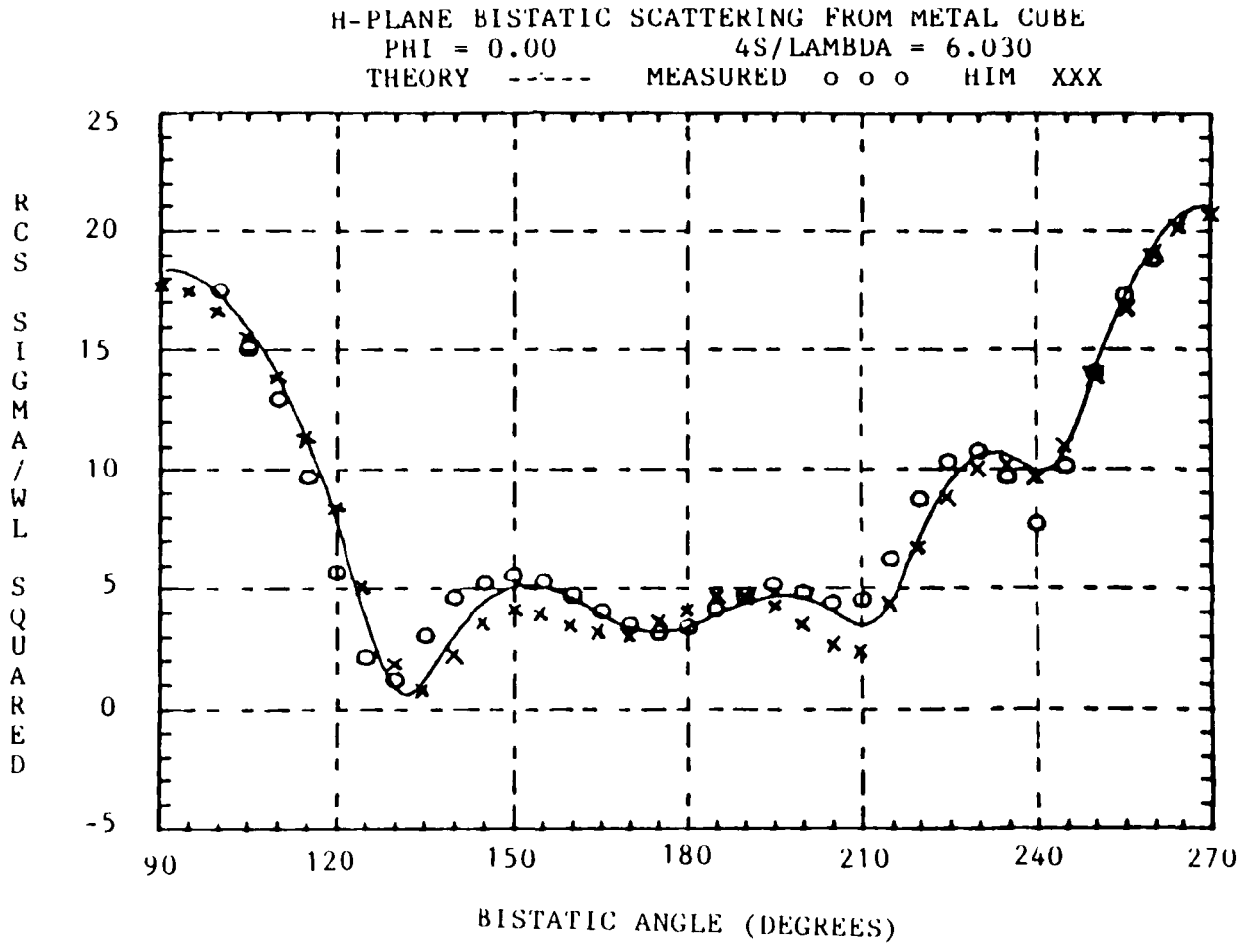

Figure 28. H-plane bistatic scattering from a metal cube 1.5λ on a side.

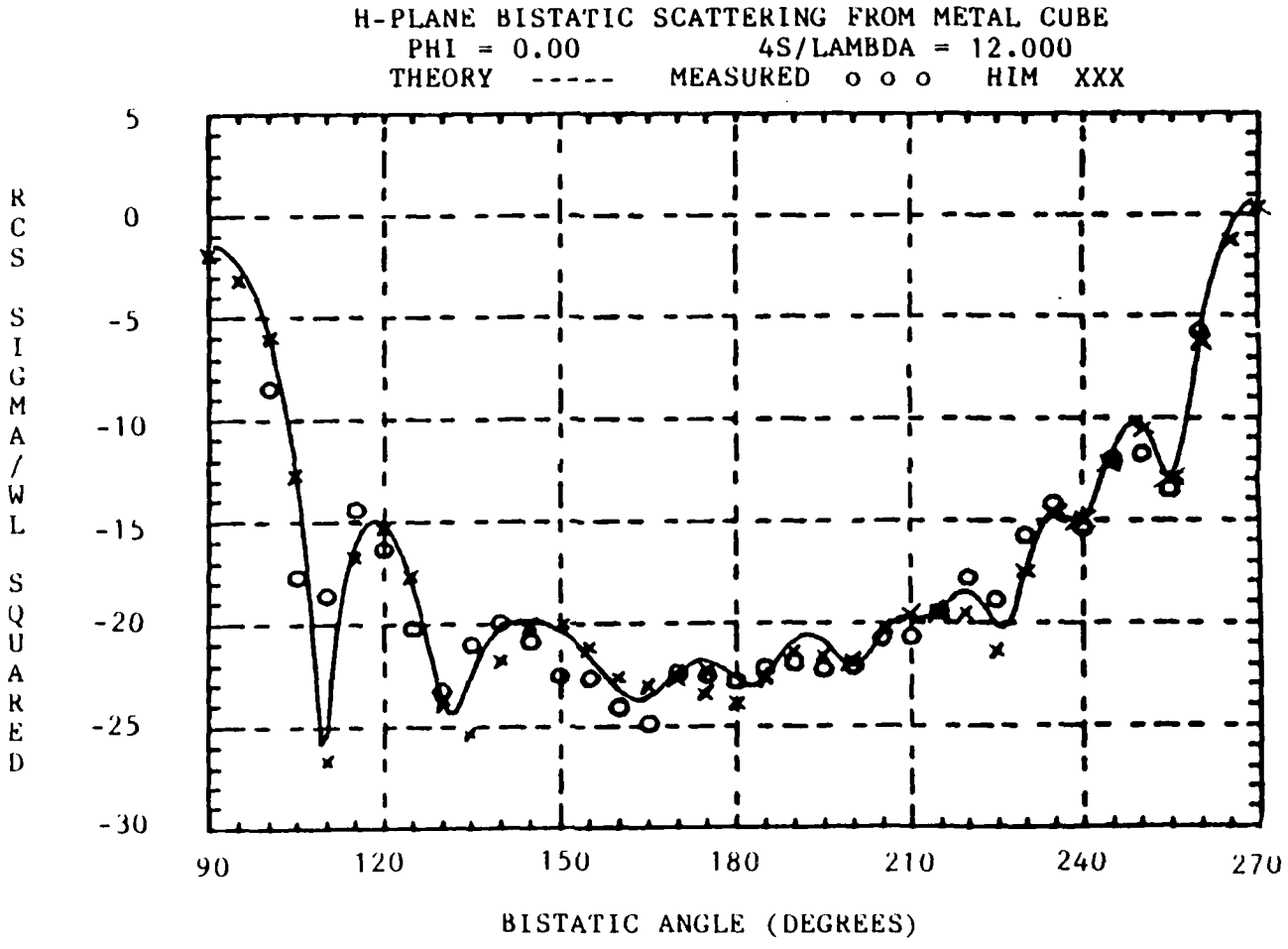

Figure 29. H-plane bistatic scattering from a metal cube 3.0λ on a side.

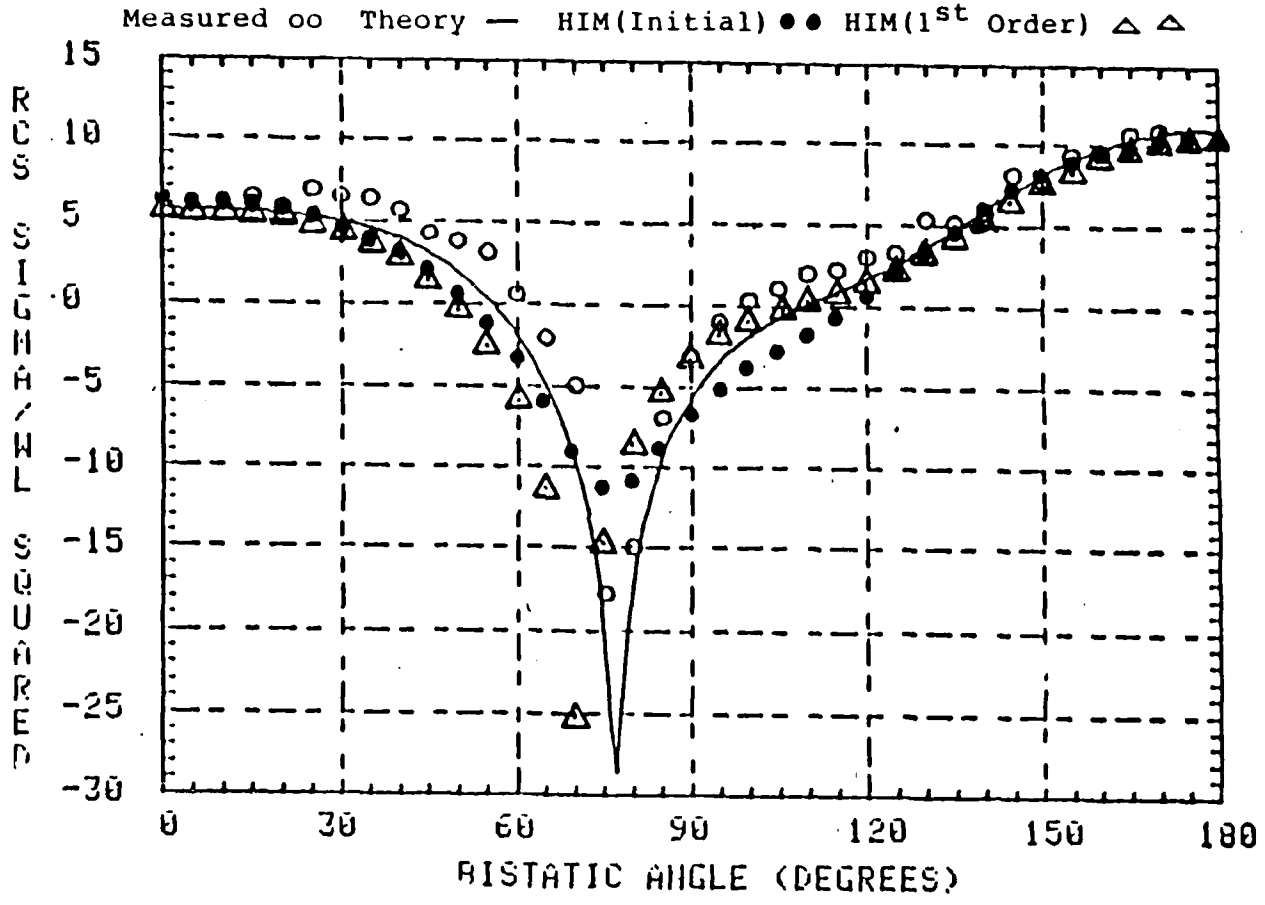

Figure 30. E-plane bistatic scattering from a metal cube of width .755 λ .

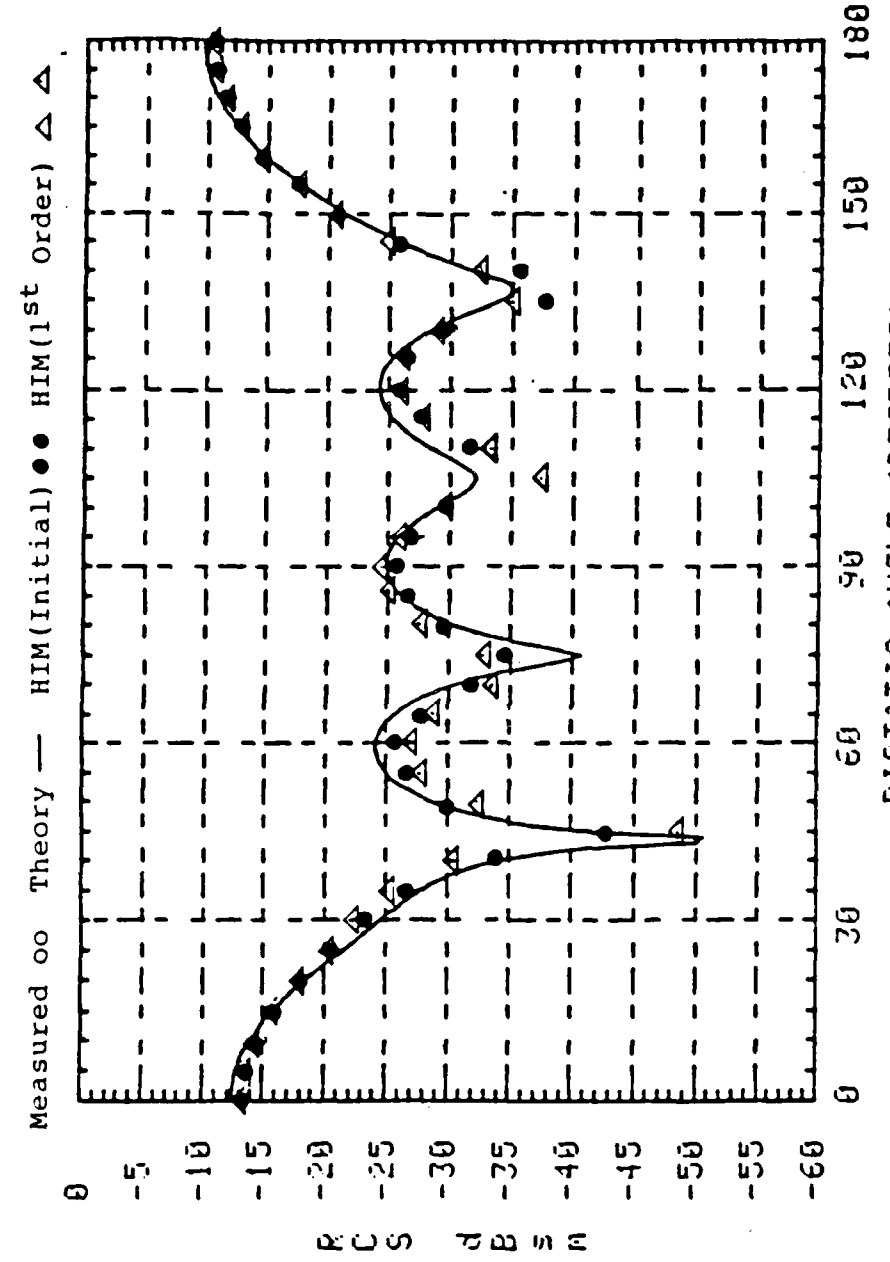

Figure 31. E-plane bistatic scattering from a metal cube of width 1.5075 λ.

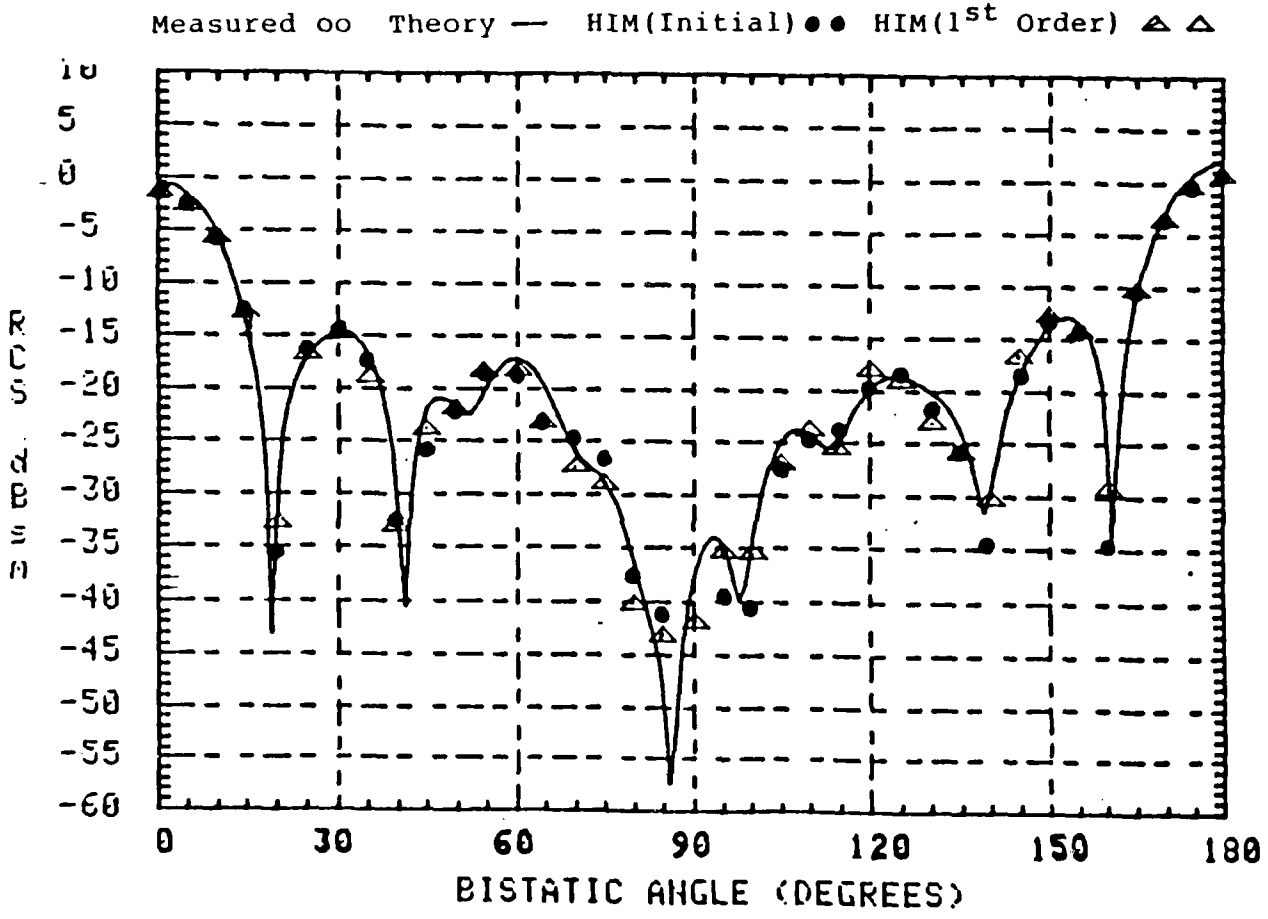

Figure 32. E-plane bistatic scattering from a metal cube of width 3.015 λ .

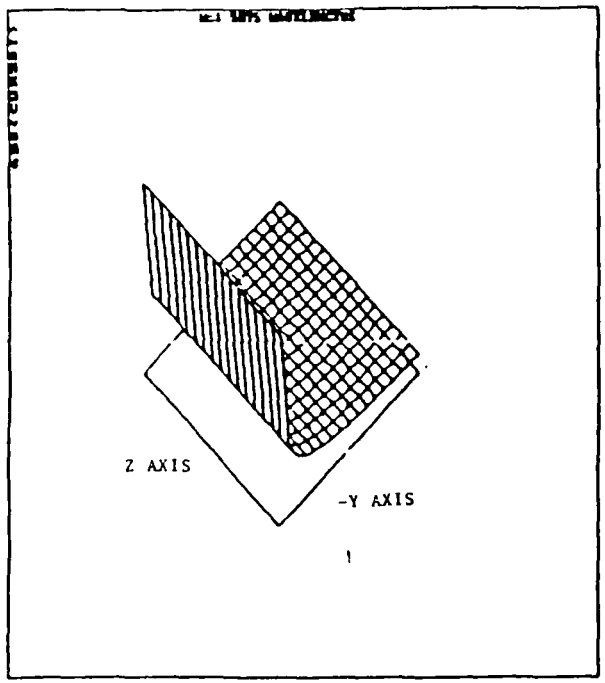

Figure 33. E-polarized component of initial current on side face - magnitude.

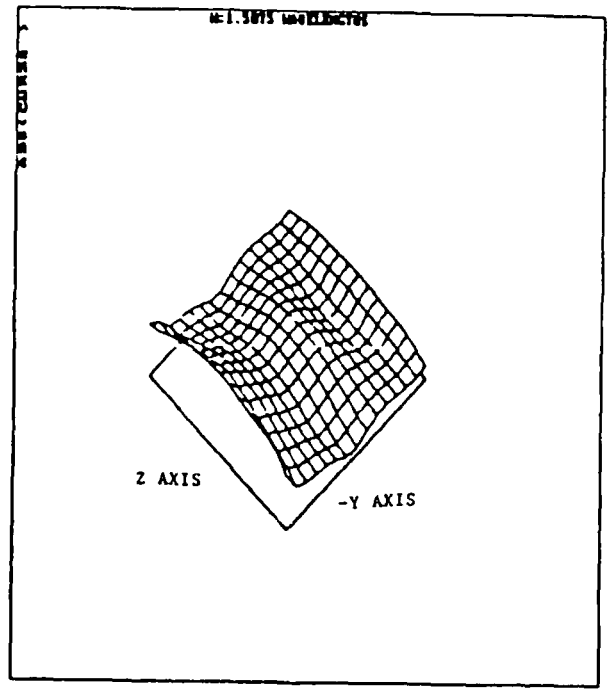

Figure 34. E-polarized component of first order current on side face - magnitude.

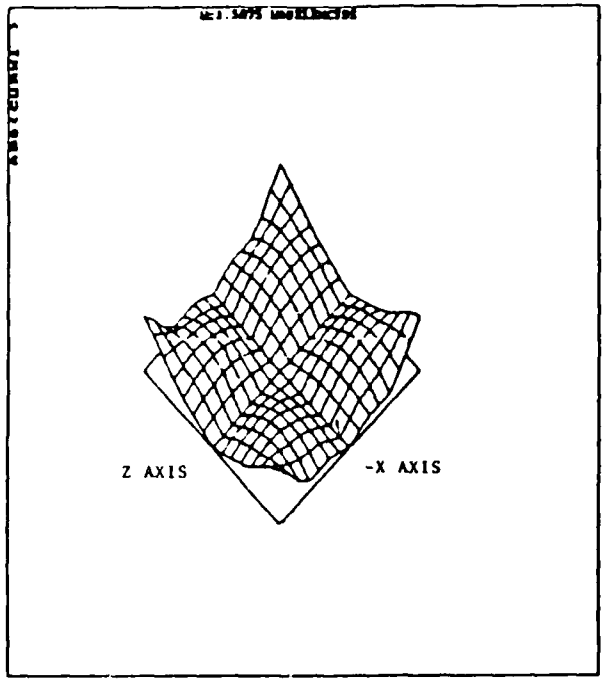

Figure 35. H-polarized component of first order current on front face - magnitude.

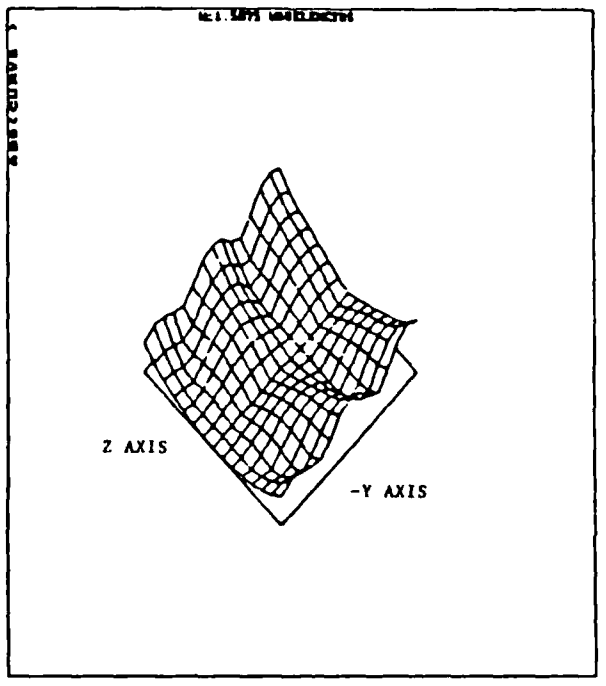

Figure 36. Cross-polarized component of first order current on side face - magnitude.

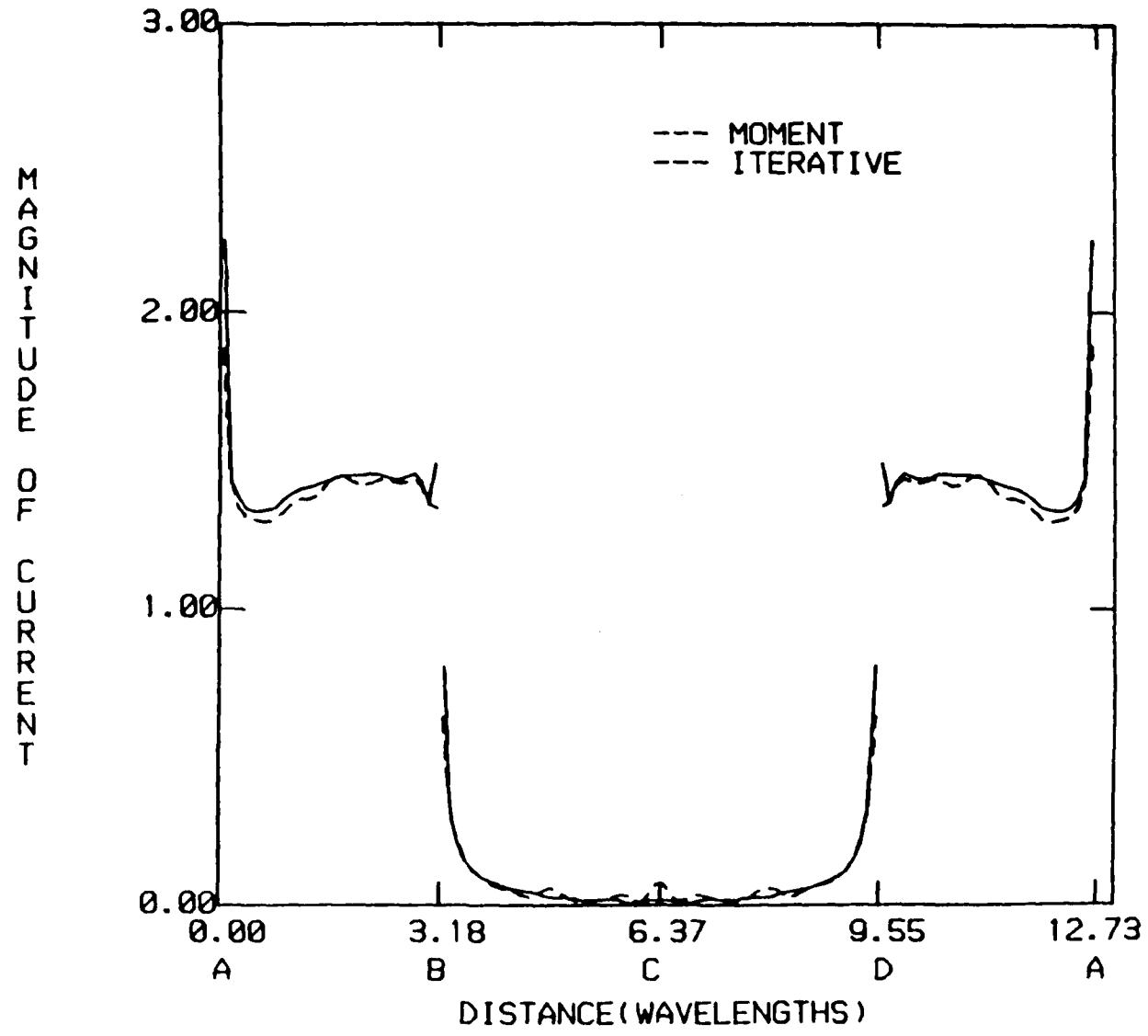

Figure 37. Magnitude of current on a square cylinder. Order = 4, $w = 3.193\lambda$, $\psi_i = 135^0$.

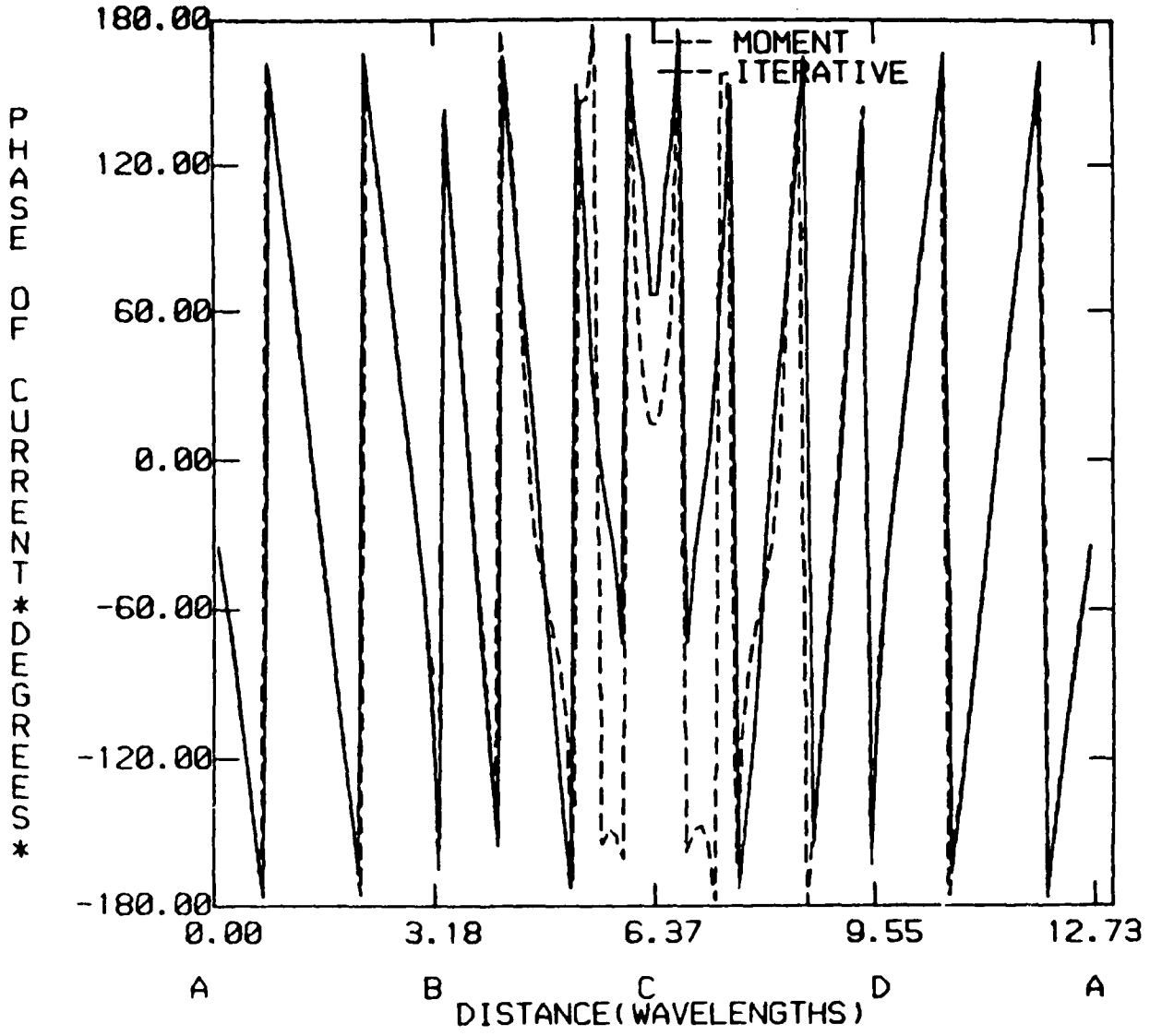

Figure 38. Phase of current on a square cylinder. Order = 4, $w = 3.193\lambda$, $\phi_i = 135^0$.

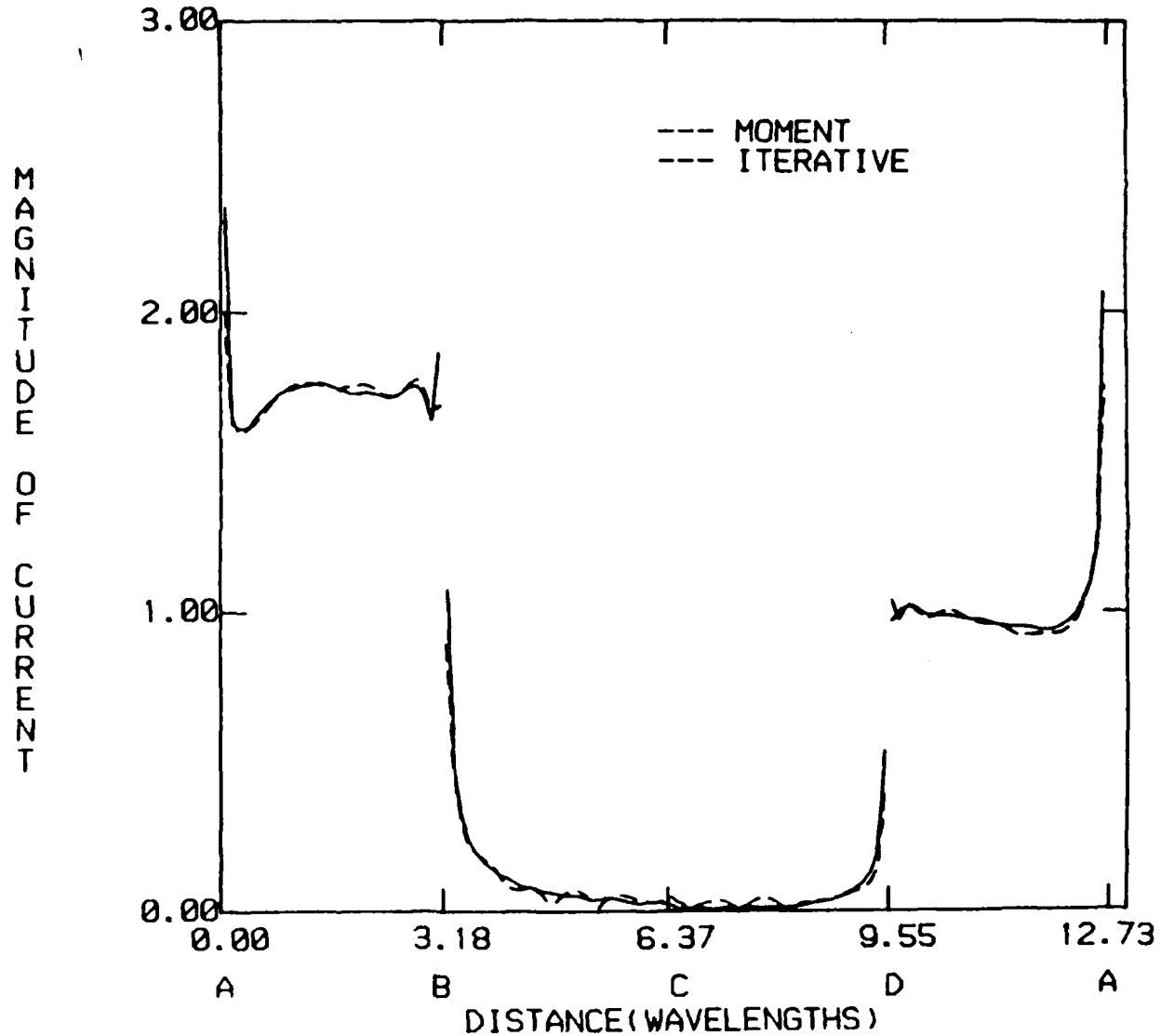

Figure 39. Magnitude of current on a square cylinder. Order = 4, $w = 3.193\lambda$, $\phi_i = 120^0$.

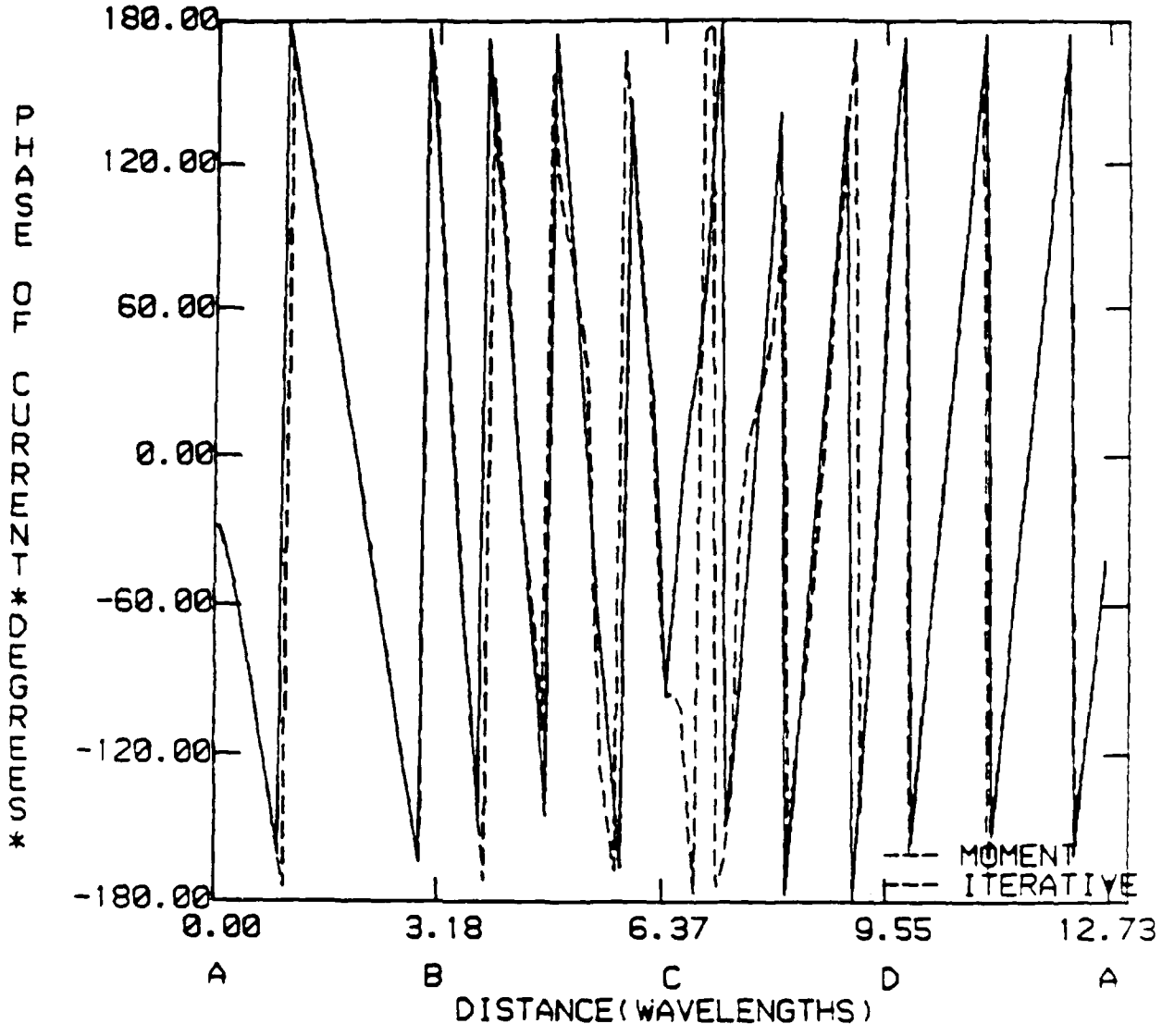

Figure 40. Phase of current on a square cylinder. Order = 4, $w = 3.193\lambda$, $\phi_i = 120^0$.

SECTION 5

SUMMARY

A new iterative method has been presented for computing the current induced by plane wave excitation on conducting bodies of arbitrary shape. In this method, the scattering body is divided into lit- and shadow-side regions separated by the geometric optics boundary. An MFIE is written for each region. Each MFIE is solved by iteration (i.e., method of successive approximations). In order to accomplish this, it is often necessary to have an initial estimate of the shadow-side current. This estimate is obtained from known physical scattering phenomena (e.g., edge diffraction theory or Fock theory). Hence, the method is called a hybrid-iterative method (HIM).

The HIM is well-suited for use on a super computer like the Cray X-MP. Results were shown for 2-dimensional objects whose size varied from 0.6λ to 440λ, all with CPU times under one minute, on the Cray. With such speed, it is possible to have a computer code with which interactive Aero/RCS tradeoffs can be evaluated.

The HIM method is a current-based approach to electromagnetic scattering. In a current-based method, the scattered field is obtained from the induced currents. This can be contrasted with the field-based approach (e.g., GTD) wherein the scattered field is obtained from the incident field via ray tracing without the necessity of explicitly determining the current. For modeling large complex geometries, it is believed that the current-based approach is better than the field based approach because one does not need to trace, perhaps, hundreds of rays and one does not need to describe geometrical surfaces to high precision.

The HIM approach to electromagnetic scattering has evolved from eight years of research sponsored primarily by RADC/Hanscom

with early support from ONR as well as lesser support from WPAFB and Rockwell Sciences Center. The merits of HIM have been well-demonstrated for perfectly conducting uncoated two-dimensional scatterers. A number of fundamental problems remain to be researched, however, before the technique can be used by the RCS community to model coated/partially coated, three-dimensional shapes.

REFERENCES

1. T. J. Kim and G. A. Thiele, "A Hybrid Diffraction Technique - General Theory and Applications," IEEE Transactions on Antennas and Propagation, Vol. AP-30, pp. 888-897, 1982.

2. M. Kaye, P. K. Murthy and G. A. Thiele, "An Iterative Method for Solving Scattering Problems," IEEE Transactions on Antennas and Propagation, pp. 1272-1279, November 1985.

3. M. Kaye, P. K. Murthy and G. A. Thiele, "An Iteration Method for Complex Scattering Problems," RADC-TR-84-204, Rome Air Development Center, New York, October 1984.

4. G. T. Ruck, D. E. Barrick, W. D. Stuart and C. K. Krichbaum, Radar Cross-Section Handbook - Volume 1, Plenum Press, New York (1970), pp. 67-94.

5. P. K. Murthy and G. A. Thiele, "Closed Form Expressions for Non-Uniform Currents on a Wedge Illuminated by a TE-Plane Wave," to appear in IEEE Transactions on Antennas and Propagation, August 1986.

6. G. L. James, Geometrical Theory of Diffraction for Electromagnetic Waves, Peter Perengrinus, Stevenage, England (1976), pp. 20-21.

7. R. F. Goodrich, "Fock Theory - An Appraisal and Exposition," IEEE Transactions on Antennas and Propagation, Vol. AP-7, December 1959, pp. 528-536.

8. P. H. Pathak, "An Asymptotic Analysis of the Scattering of Plane Waves by a Smooth Convex Cylinder," Radio Science, Vol. 14, No. 3, May-June 1979, pp. 419-435.

9. P. K. Murthy, K. C. Hill and G. A. Thiele, "A Hybrid-Iterative Method for Complex Scattering Problems," Report UDR-TR-85-56, University of Dayton, Dayton, Ohio, May 1985; prepared under Contract No. F19628-83-K-0034, AFSC, RADC/EEC, Hanscom AFB, MA.

10. L. N. Medgyesi-Mitschang, D. S. Wang, G. A. Thiele, P. K. Murthy and K. C. Hill, "Hybrid Solutions for Electromagnetic Scattering Problems," Report MDC Q1264, December 1985; prepared under AFWAL Contract No. F33615-84-C-1489, Avionics Laboratory, Wright-Patterson AFB, Ohio.

11. R. P. Penno, P. K. Murthy and G. A. Thiele, "Application of a Hybrid-Iterative Technique to a Perfectly Conducting Cube," presented at the 1986 AP-S/URSI Symposium, Philadelphia, PA, June 8-13, 1986.

12. G. H. Fallouh, P. K. Murthy and G. A. Thiele, "The Application of an Iterative Technique to Scattering by Perfectly Conducting Bodies of Revolution," presented at the 1986 AP-S/URSI Symposium, Philadelphia, PA, June 8-13, 1986.

MISSION
of
Rome Air Development Center

RADC plans and executes research, development, test and selected acquisition programs in support of Command, Control, Communications and Intelligence (C^3I) activities. Technical and engineering support within areas of competence is provided to ESD Program Offices (POs) and other ESD elements to perform effective acquisition of C^3I systems. The areas of technical competence include communications, command and control, battle management, information processing, surveillance sensors, intelligence data collection and handling, solid state sciences, electromagnetics, and propagation, and electronic, maintainability, and compatibility.